SPECIAL ISSUE ARTICLE



Check for updates

Septal deviation in the nose of the longest faced crocodylian: A description of nasal anatomy and airflow in the Indian gharial (*Gavialis gangeticus*) with comments on acoustics

Jason M. Bourke¹ | Nicole Fontenot² | Casey Holliday³

¹Department of Basic sciences, New York Institute of Technology College of Osteopathic Medicine at A-State, Jonesboro, Arkansas, USA

²New York Institute of Technology College of Osteopathic Medicine at A-State, Jonesboro, Arkansas, USA

³Department of Pathology and Anatomical Sciences, College of Medicine, University of Missouri, Columbia, Missouri, USA

Correspondence

Jason M. Bourke, Department of Basic Sciences, New York Institute of Technology College of Osteopathic Medicine at A-State, Jonesboro, AR 72401, USA.

Email: jbourke@nyit.edu

[Correction added on 6th December, after first online publication: Online open statement has been added.]

Abstract

The remarkably thin rostrum in the Indian gharial (Gavialis gangeticus) imparts challenges to nasal physiology. Competition for space in the slim jaws necessitates a thin nasal septum, leaving this taxon susceptible to nasal passage abnormalities such as septal deviation. Here we describe the nasal anatomy of gharials based on multiple individuals including one that showcases an extreme instance of nasal septum deviation. We found that gharials have both confluent nostrils and choanae, which may be important for their unique nasal acoustics. The deviated nasal septum in the female showed distinct waviness that affected the nasal passages by alternately compressing them. We performed a computational fluid dynamic analysis on the nasal passages to visualize the effects of septal deviation on airflow. Our analysis found the deviated septum increased nasal resistance and wall shear stress during respiration, resulting in unequal distribution of the air field between both sides of the nasal passage. Our findings indicate that gharials—and potentially other longirostrine crocodylians—may be particularly susceptible to septal deviations. Lastly, we observed pterygoid bullae to be present in both sexes, though their morphology differed. Airflow in the male pterygoid bullae produced a Bernoulli effect which may be responsible for the unique "pop" sounds recorded in this species.

KEYWORDS

computational, fluid dynamics, Gavialis, nasal passage, nasal septum, pterygoid bulla

Abbreviations: ant ch, anterior chamber; BL, Bourke Lab; bna, bony nasal aperture; co, concha; ch 1, primary choana; ch 2, secondary choana; cnp, cavum nasi proprium; FLMNH, Florida Museum of Natural History; lc, lacrimal; m, maxilla; nas, nasal; npd, nasopharyngeal duct; ns, nasal septum; olf, olfactory recess; OUVC, Ohio University Vertebrate Collections; pal, palatine; pmx, premaxilla; post co, postconcha; post ch, posterior chamber; preco rec, preconchal recess; prf, prefrontal; pt, pterygoid; pt bull, pterygoid bulla; rt, replacement tooth; RVC, Royal Veterinary College; UF, University of Florida; v, vomer; vest, nasal vestibule.

1 | INTRODUCTION

Indian gharials (*Gavialis gangeticus*) represent an extreme case of snout elongation and thinning, even among crocodylians (Pierce et al., 2008). Their unique cranial morphology is likely an adaptation to a largely piscivorous lifestyle (Grigg & Kirshner, 2015). Tightly constricting the

This is an open access article under the terms of the Creative Commons Attribution-NonCommercial License, which permits use, distribution and reproduction in any medium, provided the original work is properly cited and is not used for commercial purposes.

© 2021 The Authors. The Anatomical Record published by Wiley Periodicals LLC on behalf of American Association for Anatomy.

Anat Rec. 2021;1–21. wileyonlinelibrary.com/journal/ar

width of their tubular rostrum decreases drag through the water when the rostrum is quickly moved through a horizontal plane (McHenry et al., 2006), allowing for rapid acceleration through the water when hunting agile prey. However, snout elongation and tubular compression does incur costs, especially to bite force and skull stress (Erickson et al., 2012; McHenry et al., 2006). Constricting the width of the rostrum limits the available space for structures residing inside it, such as replacement teeth and the nasal passages. In the case of the latter, this space limitation may make gharials more vulnerable to nasal pathologies such as deviation of the nasal septum.

The nasal septum serves as the primary separator of the two parallel nasal passages (Takahashi, 1987). The nasal septum has been implicated as an inducer of splanchnocranium growth in some mammals (Copray, 1986; Takahashi, 1987). Bridging the vertical space between the dorsal and palatal sides of the skull, the nasal septum provides important structural support for the skull when biting (Moss, 1976). Crocodylians further incorporate the nasal septum into structural support via a mixed collagenous and elastic fiber longitudinal tension chord that runs the length of the base of the nasal septum within a U- or V-shaped, trenchant base known as the septal sulcus (Klenner et al., 2016). The extra bracing provided by this tension cord suggests that nasal septum rigidity may be more important for crocodylians than most other amniotes and that septal deviations may be particularly deleterious for these reptiles.

By reducing the size of the rostrum, gharials limited the potential of the jaw to contribute to acoustic communication behaviors common to crocodylians, such as head slapping and jaw claps (Dinets, 2013). These limitations may explain why gharials are considered the quietest of extant crocodylians (Dinets, 2013; Grigg & Kirshner, 2015). The evolution of the fleshy, hollow ghara in large males and expansion of the pterygoid sinus into an enlarge bulla (pterygoid bulla) appear to be methods by which gharials were able to retain an acoustic presence while still reducing the breadth of the rostrum. The rostrally placed ghara has been observed emitting a distinctive buzzing sound (Dinets, 2013) in large males during courtship, solidifying its function as a primary acoustic structure. Whereas the caudal location of the pterygoid bulla and its enlarged, hollow shape indicates that this structure may function as a resonating chamber for sound (Martin & Bellairs, 1977). To date, this hypothesis has been based on the skeletal morphology of the bulla and its relationship to the surrounding nasal anatomy.

Herein, we describe the nasal anatomy and airflow patterns of *G. gangeticus* based on multiple specimens. One specimen was a large adult female that presented with a unique instance of septal deviation never before documented in an amniote. We compare nasal passage shape to other gharial specimens and other crocodylians

to determine potential effects of this septal deviation. We perform a computational fluid dynamic (CFD) analysis on the nasal passages of the female with the deviated septum and a large male with a more typical (though still slightly deviated) septum. We describe the general pattern of airflow during both phases of resting respiration and compare airflow patterns between these two specimens to assess the potential physiological consequences of septal deviation in *Gavialis*. Lastly, we looked at airflow through the pterygoid bulla in relation to its potential function as an acoustic resonator.

2 | MATERIALS AND METHODS

2.1 | Specimens

We were granted access to three gharial specimens (G. gangeticus) for this study. The specimen with the deviated septum was an approximately 50-year-old, 310-cm adult female that passed away at the Fort Worth Zoo (TNHC 110000, hereafter referred to as Louise). The specimen had perished in captivity and was given a diceCT treatment (Gignac et al., 2016) by the Holliday Lab. The use of diceCT allowed for a detailed analysis of the entire nasal passage. Reference specimens included a 39-year-old, 365-cm adult male from the St. Augustine Alligator Farm (SA91285, hereafter referred to as Taj) and the dried skull of a large adult individual of unknown sex from the Florida Museum of Natural History (UF118998). The total length of UF118998 was estimated using a head length: total length ratio of 1:6.5 (Whitaker & Whitaker, 2008). This produced an estimated total length of 346 cm. Other crocodylians used for reference included adult specimens of Melanosuchus niger (RVC-JRH-FBC1), Alligator mississippiensis (BL-007), and Crocodylus johnstoni (OUVC 10425). We looked at juvenile specimens of Crocodylus porosus (OUVC 10899) and C. johnstoni (OUVC 10426). Gharial specimen, UF118998 was obtained from the Florida Museum of Natural History Herpetology Collections via the Morphosource website (Morphosource. org. Morphosource ID: 000039794). C. porosus specimen was obtained from the WitmerLab via Morphosource (ID: 000S22084). The C. johnstoni specimen was obtained from the WitmerLab and Data Dryad (https://doi.org/10.5061/ dryad.mt64k). The M. niger specimen was obtained from the CrocBase website (Hutchinson, John R, and Lauren H Sumner-Rooney. 2016. "Melanosuchus Niger RVC-JRH-FBC1 Head." OSF. June 17. osf.io/qgmpf.).

2.2 | Three-dimensional models

Scan data (DICOM or TIFF format) were imported into the three-dimensional (3D) visualization and analysis

as "zones" or "parts" that the engineering software could

recognize, allowing for granular volumetric "shrinkwrap"

meshing using the meshing utility in ANSYS Fluent 2019

R2 (ANSYS, Inc., Canonsburg, PA). Volumetric meshes

were made using the mosaic method in Fluent. This

involves a polyhedral-hexahedral mesh generation. The

ability of polyhedral cells to accurate capture complex geometry makes them particular appealing for biological

systems (Bass et al., 2019; Speigel et al., 2009). The high

node: face ratio for each cell, allowed accurate gradient resolution at relatively low volumetric cell counts

(Sosnowski et al., 2018) and without the warping issues

the vestibule-CNP junction up to the secondary choana (Figure 1). The secondary choana in all of our gharials specimens was a shared opening between both nasal pas-

sages (see Section 3), allowing the use of a singular inlet/outlet boundary to be placed on it. The nasal vestibule

was omitted in both gharial specimens as postmortem constriction obscured the shape of this region of the nasal

passage and proved challenging to accurately segment

The complete, bilateral, nasal passages of gharials, Louise and Taj were reconstructed from the CT data. These nasal passages incorporated all the geometry from

associated with other modeling methods.

software, Avizo Lite 2019.1 (Thermo Fisher Scientific, Waltham, MA). Skulls and airways for each animal were segmented into 3D models for analysis in the program. Airway models of the gharial specimens were exported as Standard Tessellation Language (STL) files where they were imported into the engineering and 3D printing software, Geomagic (3D Systems, Rock Hill, SC) where the models were cleaned of segmentation artifacts (e.g., skewed triangles, spikes, and small holes) and prepared for volumetric meshing. The cleaned STL files were returned to Avizo where boundary IDs were painted on them using the surface editor tool. These IDs functioned

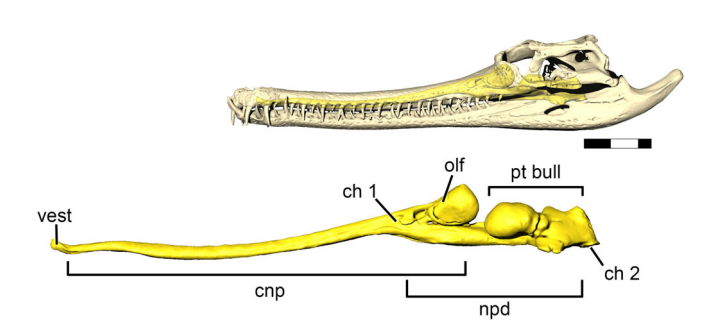


FIGURE 1 Sagittal view of nasal passage anatomy in *Gavialis gangeticus* (SA91285). Scale bar = 10 cm. ch1, primary choana; ch2, secondary choana; cnp, cavum nasi proprium; npd, nasopharyngeal duct; olf, olfactory recess; pt bull, pterygoid bulla; vest, nasal vestibule

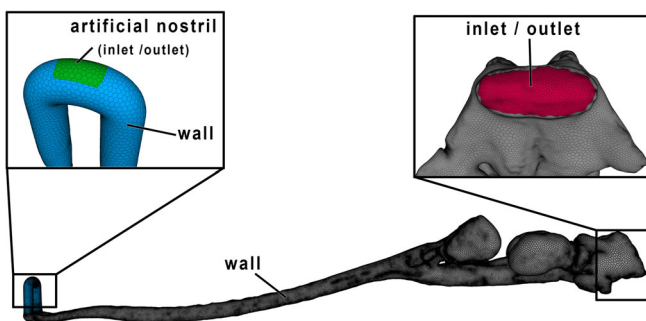


FIGURE 2 CFD model for Taj (SA91285) showing the boundary condition assignments. Insets show the artificial nostril at the rostral end and the secondary choana (ventral view) at the caudal end

without inducing artifacts that negatively impacted model performance. To avoid artificial imbalances at these inlets caused by their slightly different geometries, an artificial nasal vestibule with a single inlet/outlet was attached to the model (Figure 2). These models ensured a balanced influx and efflux of air through the nasal vestibule and proved to have an anatomical basis as we observed confluent nostrils in both gharial specimens (see Section 3). Data from these artificial extensions were not recorded and the artificial nostril was omitted from most figures to avoid confusion.

2.3 | Respiratory variables

To determine tidal volume and respiratory drives, we needed to know the masses of our gharial specimens. To determine the approximate mass values for our specimens (Table 1), we used two different mass estimate equations (Khadka & Bashyal, 2019; Maskey, 1989):

TABLE 1 Mass estimates based on total length in gharial specimens

Specimen	Skull length (cm)	Total length (cm)	Mass (kg) ^a	Mass (kg) ^b
Louise	43.41	310	50.75	174.51
Taj	54	351	61.89	198.01
UF118998	50.53	328.38	55.74	185.05

^aKhadka and Bashyal equation.

^bMaskey (1989)) equation.

$$mass(g) = -3115.59 + 573(TL),$$

$$mass(kg) = 0.2719(TL) - 33.544,$$

where TL is the total length in centimeters.

Both equations were empirically derived from multiple measurements of hatchling (Maskey, 1989) and juvenile gharials between 4 and 6 years of age (Khadka & Bashyal, 2019). To estimate tidal volume, inspiratory and expiratory drives, we used the empirically derived equations for mass-dependent resting respiration in alligators (Farmer, 2006; Farmer & Carrier, 2000).

$$V_T = 20.7 M^{1.06} (ml),$$

Inspiration = $370 \,\text{ml/kg/min}$,

Expiration = $369 \,\text{ml/kg/min}$.

Resistance was calculated using the standard equation:

$$R = \frac{\Delta P}{Q},$$

where ΔP is the change in pressure from atmosphere to choana (= the pressure drop), and Q is the flow rate in ml/s (Vogel, 1994).

Wall shear stress for a Newtonian fluid can be calculated from the equation

$$\tau = \mu \frac{\partial U}{\partial n}$$
,

where μ is the dynamic viscosity (kg/ms), U is the flow velocity normal to the wall, and n is the distance from the wall (Vogel, 1994).

2.4 | Computational fluid dynamics

Fluid dynamic analysis was performed using the CFD package, Fluent 2019 R2 (ANSYS, Inc., Canonsburg, PA). Models were run using a quasi-steady state condition. This conditions assumes a direct relationship between the instantaneous flow rate and pressure gradient of the flow field (Loudon & Tordesillas, 1998). Quasi-steady assumptions are viable for instances in which the air field assumes the typical parabolic flow profile. This is commonly observed under low Reynolds and Womersley number conditions such as resting respiration (Bourke et al., 2014, 2018; Craven et al., 2009; Jiang & Zhao, 2010).

To verify the quasi-steady state, we performed a cross sectional analysis of the airway (Bourke et al., 2014). Calculated Reynolds and Womersley numbers indicated that airflow should be quasi-steady through the nasal passage, with much of the flow field existing in the transitional zone between laminar and turbulent flow (Table 2). To accommodate this potential for turbulence, we used the Wilcox two equation κ - ω turbulence model, with an additional shear stress transport and low Reynolds correction additions. This approach provides good approximations for the dynamics of airflow in transitional flows (Chen et al., 2009; Li et al., 2017; Liu et al., 2007). To ensure physiologically realistic flow patterns, we assigned a pressure inlet boundary at the nostrils for inspiration and the secondary choana for expiration. This boundary condition had static pressure equal to atmospheric (gauge) pressure. We assigned a pressure outlet boundary condition to the secondary choana for inspiration and the nostrils for expiration. The volumetric flow rate (ml/s) was converted to mass flow rate (kg/s) at the pressure outlet and the program was allowed to vary the pressure profile at the outlet as needed to achieve the desired flow rate, creating the pressure gradient that drove movement of air through the nasal passages.

Models ran until the residuals of error for continuity, momentum and turbulence had reached $1.0e^{-4}$ or lower (convergence). We used surface monitors placed throughout the nasal passage to better assess convergence of each model. The asymptotic "flattening" of values at these surface monitors between iterations provides a more granular metric for monitoring convergence and potential problem regions in the models. Surface monitors were placed within the CNP, olfactory recess, and nasopharyngeal duct on both sides of the nasal passage.

2.5 | CFD postprocessing

We used the ANSYS CFD postprocessing package, EnSight 2019 R2, to visualize the flow data. General flow patterns were visualized using particles produced from 100 seeds located at specific locations within the airway (often from the inlet, but occasionally from cross sections located near areas of interest such as the olfactory recess

TABLE 2 Range of calculated Reynolds and Womersley numbers for the airways in Louise and Taj low-end and high-end estimates based on calculated flow rates using masses from Table 1

Specimen	Reynolds number	Womersley number
Louise	1,336-2,731	1.1-2.04
Taj	1,358-4,074	0.76-1.3

or anterior chamber of the pterygoid bulla). Massless particles were seeded and allowed to run throughout the remainder of the nasal passage, highlighting pathlines and providing a qualitative measure of the air field during each modeled phase of respiration. To obtain volumetric flow rates we took a series of six to eight cross sections from regions of interest (e.g., the olfactory recess). The distance between each cross section was 4–5 mm. Flow rate was calculated for each cross section using the standard flow rate equation:

$$O = \overline{V}A$$
.

where Q is the flow rate (m³/s), \overline{V} = the average velocity magnitude in the rostrocaudal direction (m/s) and A is the area of the cross section (m²). Flow rates were converted into milliliters for ease of comparison. To reduce over and underestimation of flow due to standing vortices and other recirculation events that may have been captured in a single cross section, we used the average flow rate values from the sum of our six to eight slices.

2.6 | Mesh refinement

A mesh refinement study was performed to ensure mesh independence. Mesh refinement was performed using meshes of different resolutions, with values of interest (e. g., pressure) monitored between meshes using a spline placed at the same location within each model. This provided an accurate means of capturing data from the same location for each model resolution, allowing for direct comparisons and quantification. Data were plotted together to compare changes in magnitude between models.

2.7 | Septum measurements

We measured the width of the nasal septum in each crocodylian specimen based on axial CT slices starting from the primary choana and extending rostrally to the nasal vestibule. We focused on this region as this was the location of nasal septum deviation (see Section 3). Septa were measured in three places at each location: the top of the septum near the roof of the nasal cavity, the middle of the nasal septum, where the structure was typically thinnest, and the base of the nasal septum near the septal sulcus. For Louise, we measured the straight-line distance from the angle of the septum's deviation. We measured full nasal passage width (distance between the lateral walls of both nasal passages) at these same

locations to calculate the percentage of the nasal passage occupied by the nasal septum for each specimen. CT quality varied from specimen to specimen, limiting the number of informative slices that could be obtained along the rostrum (range: 6–22 slices/specimen). In general, longer snouted taxa had more available CT slices than shorter-snouted taxa. This was largely coincidental, as all of our longer snouted specimens happened to also have higher resolution CT scans, whereas many shorter snouted specimens came from full-body scans with increased acquisition field of view and consequently, lower overall resolution.

3 | RESULTS

3.1 | Mesh independence

Results of our grid refinement study found that a grid resolution between 2.4–3.6 million elements was sufficient to produce mesh independence for both gharial specimens (Figure 3). These element numbers gave the models an average poly-hex cell size of 29–92 µm.

3.2 | Crocodylian nasal anatomy

Crocodylians share the same basic nasal anatomy as other amniotes (Figure 1; Parsons, 1970). The opening of the naris to the duct of the nasal gland, referred to as the nasal vestibule, is very short, descending from the naris to the floor of the nasal passages before sharply turning caudally to give way to the nasal cavity proper, or cavum nasi proprium (CNP, Figure 1). This is the largest proportion of the nasal passage in crocodylians. It houses three conchae (mucosa covered invaginations of the nasal walls), the preconcha, concha, and postconcha. The latter two conchae reside in a specialized region of the nasal passage called the olfactory recess. This area of the nasal passage is removed from the main air field, producing a relatively high static pressure, cul-de-sac in the nose that reduces the speed of respired air, providing time for odorant molecules to be captured by olfactory receptors (Mozell & Jadodowicz, 1973). A well-developed olfactory recess is associated with macrosmia (Craven et al., 2010). The junction between the olfactory recess and the remainder of the CNP is called the primary choana (Figure 1), as this region of the crocodylian nose is homologous with the choana of other amniotes (Witmer, 1995). The remainder of the nasal passage—inferior and caudal to the olfactory recess-continues in a greatly elongated tube called the nasopharyngeal duct. This structure extends for almost the same distance caudally as the rest

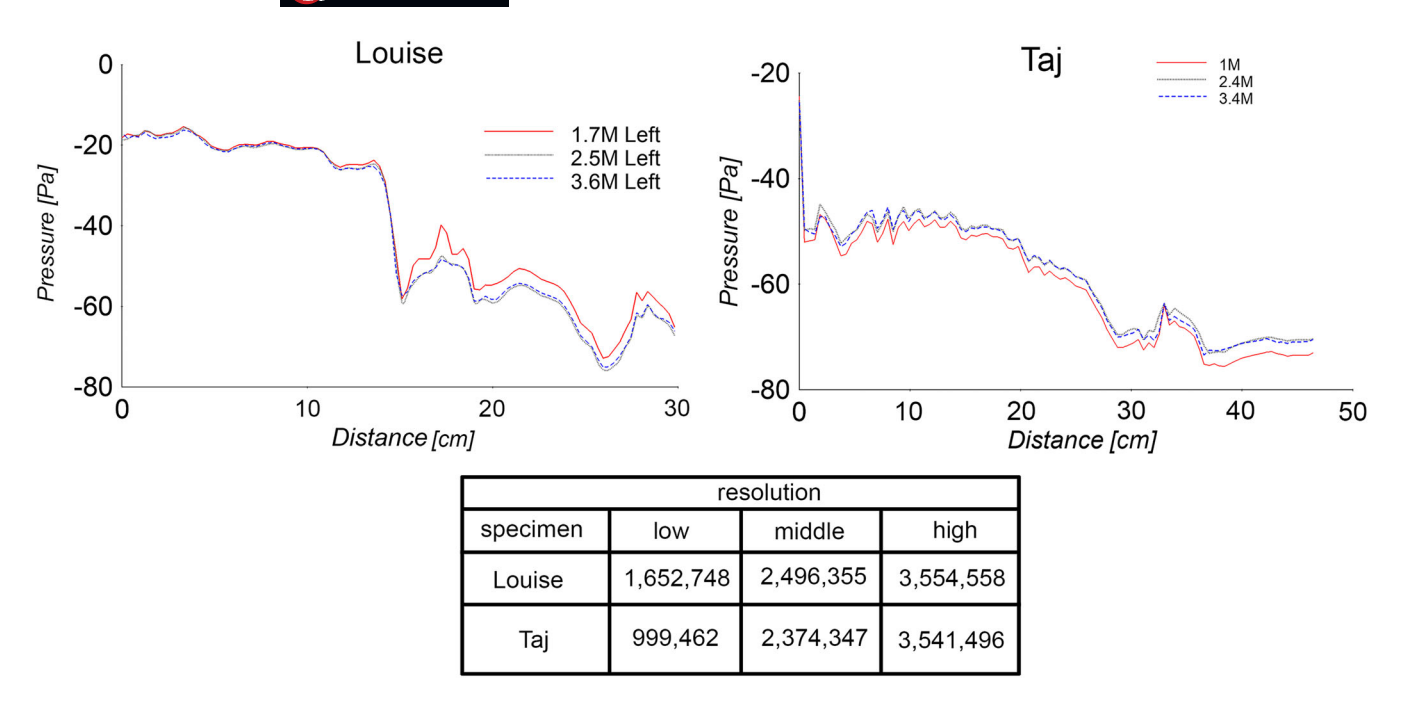
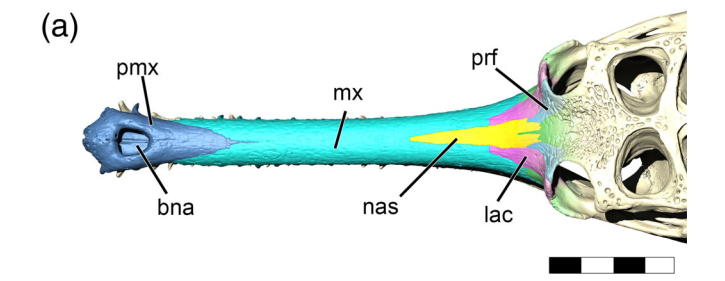


FIGURE 3 Grid refinement results graphed for each gharial specimen

of the nasal passage does rostrally (Figure 1). The nasopharyngeal duct terminates at an opening in the pterygoids, the secondary choana. From here, the nasal passages connect to the glottis and trachea to conduct air to the lungs.

3.3 | Gharial-specific nasal anatomy

Similar to other crocodylians, the nasal cavity of Gavialis incorporates portions of the premaxillae, maxillae, palatines, pterygoids, vomers, nasals, prefrontals, frontals, and lacrimals (Figure 4; Witmer, 1995). Caudal to the primary choana, bony contributions to the nasal cavity include the palatines, which provide the floor and lateral walls to the nasopharyngeal duct. The vomers form the roof of the nasopharyngeal duct initially before they are replaced by the pterygoids, which completely encase the secondary choana (Figure 4b). The lacrimals, prefrontals, frontal, nasals, and maxilla form the walls and ceiling of the olfactory recess. In all our specimens, caudal to the olfactory recess, the roof of the nasopharyngeal duct expanded into an enlarged pterygoid bulla (Figure 5; Martin & Bellairs, 1977; Hone et al., 2020). The pterygoid bulla can be divided into two parts. The first and most noticeable part is the anterior chamber (Figure 4; Martin & Bellairs, 1977). It consists of an enlarged, egg-shaped structure with an ostium that communicates with the nasopharyngeal duct. The posterior chamber is a smaller, less defined structure that drains into the secondary choana. The two chambers are separated from each other



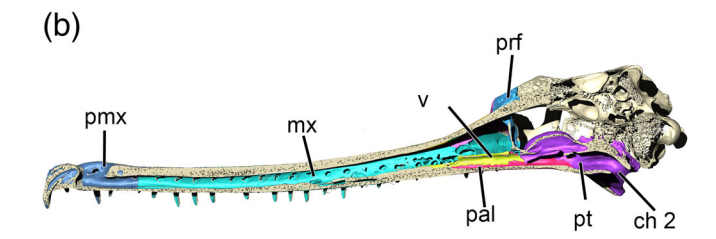


FIGURE 4 Nasal cavity in *Gavialis gangeticus* (UF118998) in dorsal view (a) and with a midsagittal cross section (b). Bones are colored to show contributions to nasal cavity. Scale bar = 10 cm. bna, bony nasal aperture; ch2, secondary choana; lac, lacrimal; mx, maxillae; nas, nasals; pal, palatine; pmx, premaxillae; prf, prefrontal; pt, pterygoid; v, vomer

by a constriction in the pterygoids (Figure 5; Martin & Bellairs, 1977).

Bony contributions to the nasal cavity rostral to the primary choana show some departure from other crocodylians. Most notably, the nasal bones in *Gavialis* are reduced compared to both crocodylids and alligatorids (Figure 5a). In the former two families, the

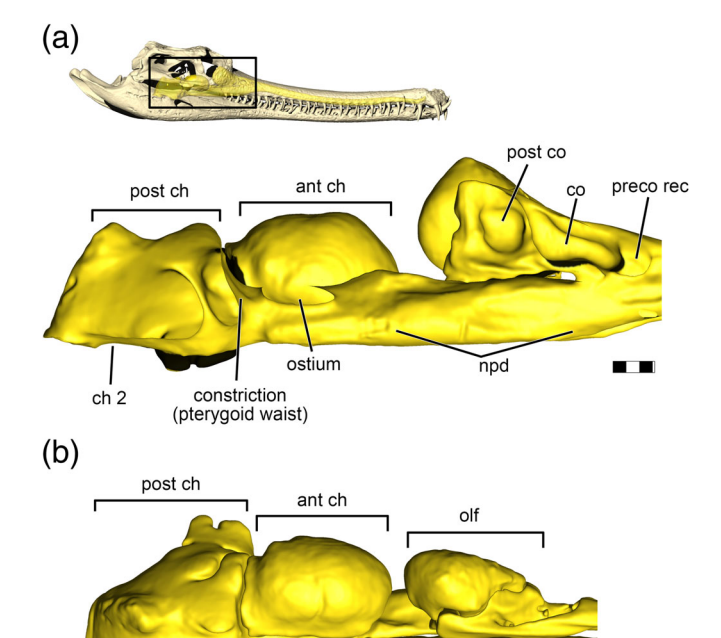


FIGURE 5 Olfactory recess and pterygoid bullae in midsagittal (a) and dorsal (b) aspects for *Gavialis gangeticus* (SA91285). Scale bar = 1 cm. ant ch, anterior chamber; ch2, secondary choana; co, concha; npd, nasopharyngeal duct; olf, olfactory recess; post ch, posterior chamber; post co, postconcha; preco rec, preconchal recess

npd

constriction

(pterygoid waist)

bony nasal aperture ("bony nostril") is comprised of the premaxilla, maxillae, and nasals. In alligatorids, the nasals terminate in a substantial spine that separates the bony nasal aperture into left and right sides. In crocodylids, the nasals extend into the terminal spine, but the spine does not traverse the bony nasal aperture and instead forms the caudal border of the aperture. In contrast, the bony nasal aperture in *Gavialis* is entirely comprised of the premaxilla, which further extends caudally several millimeters before giving way to the two maxillae (Figure 4a). Dorsally, the nasals disappear approximately one-third the rostral distance from the primary choana (Figure 6a). Ventrally (along the roof of the nasal cavity), the nasals continue rostrally to approximately the halfway point between the primary choana and the tip of the snout (Figure 6a).

The vomers in *Gavialis*, caudal to the primary choana, are consistent with other crocodylians (Romer, 1956; Witmer, 1995). Rostral to the primary choana, the contribution of the vomer to the nasal cavity is reduced as rostrum lengthening is comprised mostly of the maxillae and premaxillae (Figure 6b). This relationship is similar

to that observed in crocodylids (Figure 6b). In contrast, the vomers in alligatorids continue rostrally from the primary choana anywhere from half the length to the entirety of the rostrum (Figure 6b), and even form a substantial part of the nasal cavity floor in the alligatorid, *M. niger* (Vieira et al., 2016).

3.4 | Nasal anatomy of Louise (TNHC 110000)

From the nostril to the secondary choana, the straightline length of the nasal passage was 425.74 mm. The tip of the rostrum had a slight lateral deviation to the left side (Figure 7a). The nostril was a single, confluent opening where air entered from the environment. This confluence continued 12 mm deep to the nostril where the nasal passages diverged into left and right nasal vestibules that descended a short distance before curving into the CNP (Figure 7b). Septal deviation produced a horizontal wave that extended from the junction of the CNP and nasal vestibule and ended approximately 60 mm rostral to the primary choana (Figure 7a). Comparing the nasal passage to the nasal cavity revealed that the septal sinuosity began shortly after the disappearance of the vomer. The sinuous nasal septum in Louise produced five waves of the CNP. Amplitude and frequency of septal waves stayed consistent, save for the first proximal wave and the final, distal wave (Figure 7a). The nasal vestibule showed no evidence of septal deviation, nor did the remainder of the nasal passage caudal to the primary choana. The olfactory recess was similar to crocodylids, in which the concha and postconcha are aligned in succession to one another (Witmer, 1995). Inferior to the olfactory recess, the nasopharyngeal duct continued caudally from the primary choana 74 mm before opening into the expanded anterior chambers of the pterygoid bullae. The distance between the caudal terminus of the olfactory recess and rostral limit of the pterygoid bullae was 12 mm. Upon expansion of the pterygoid bullae, the nasal septum terminated, making both nasal passages confluent for the remainder of their course. The anterior chambers of the bullae in Louise were large, shallow oblong cavities that extended from the roof of the nasopharyngeal duct and partially wrapped around the sides (Figure 8a). The ostia for the anterior chambers were wavy ellipses 11.7 × 23.5 mm wide, that opened at approximately a 41° angle from the center of the air field of the nasopharyngeal duct (Figure 8a). At their widest, the anterior chambers of the bullae covered a distance of 32 mm on each side. Caudal to the ostia, the nasopharyngeal duct continued for another 51 mm, passing through a slight constriction of the pterygoids before opening into



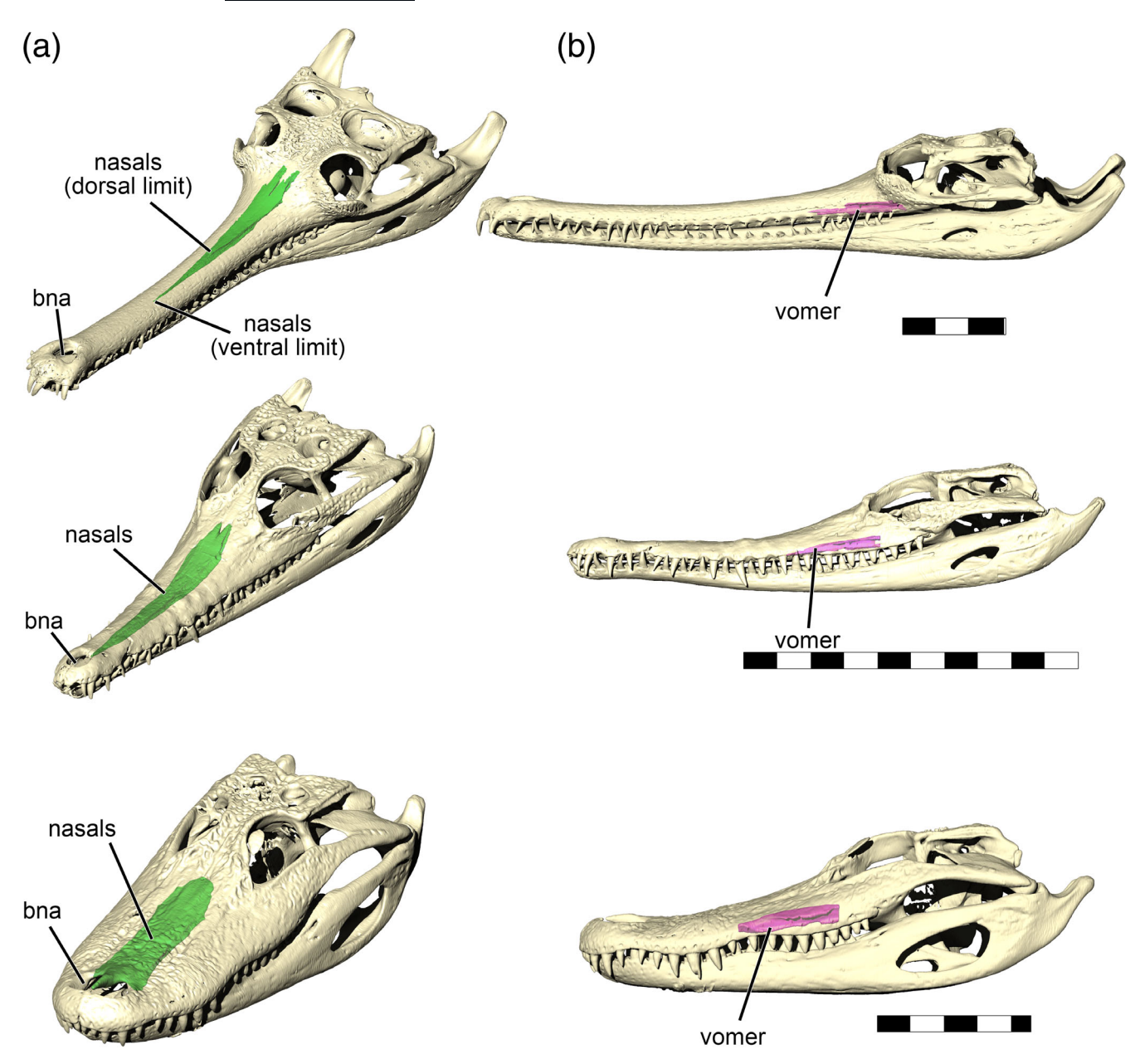


FIGURE 6 Relative contributions of the nasals (a) and vomers (b) to the nasal cavity in *Gavialis gangeticus* (top), *Crocodylus johnstoni* (middle), and *Alligator mississippiensis* (bottom). Scale bar = 10 cm. bna, bony nasal aperture

the enlarged posterior chamber. The posterior chamber was a large, confluent structure that expanded around the nasopharyngeal duct and ended at the secondary choana. In spite of the lack of a nasal septum in this region, the floor of the nasopharyngeal duct retained two shallow troughs for each nasal passage.

3.5 | Nasal anatomy of Taj (SA91285)

From nostril to secondary choana, the straight-line length of the nasal passage was 476.89 mm. Although

this specimen was a mature male, it only had a small and fairly subdued ghara (Figure 9b). As with Louise, the ghara opened to a single, confluent nostril that remained confluent for approximately 10 mm before the nasal passages properly diverged. However, unlike Louise, distinct channels could be seen in the developing ghara of Taj (Figure 9b). These channels would have guided air into their respective nasal passages, reducing mixing in this region. Deep to the ghara, the separate nasal vestibules descended and joined with the CNP. A similar series of horizontal waves to Louise was observed in Taj. However, the extent of the sinuosity was more reduced, with

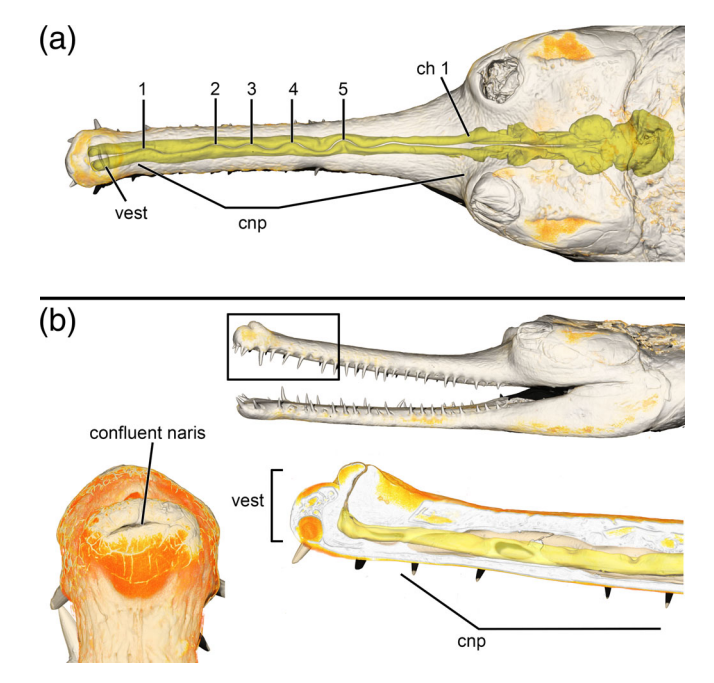


FIGURE 7 Nasal passages of Louise (TNHC 110000). (a) Dorsal view of nasal passage showing the individual waves of the CNP (numbers). (b) Midsagittal view of the nasal vestibule and CNP, with dorsal view of the confluent naris. cnp, cavum nasi proprium

only three shallow waves observed (Figure 9a). These waves occurred caudal to the nasal vestibule and terminated 166 mm rostral to the primary choana (Figure 9a). As with Louise, septal sinuosity was present rostral to the disappearance of the vomer. The olfactory recess retained the same morphology observed in Louise. The nasopharyngeal duct ran 77 mm caudal from the primary choana before opening up into the anterior chambers of the pterygoid bullae. The distance between the end of the olfactory recess and the pterygoid bullae was shorter (≤10 mm) than what we observed in Louise. The anterior chambers of the pterygoid bullae in Taj were bulbous and more strongly rounded compared to Louise (Figure 8b). The ostia of the anterior chambers were well defined and formed ellipsoidal entrances 11 × 25 mm in diameter in the roof of the nasopharyngeal duct. These ostia were angled approximately 48° from the free stream region (Figure 8b). At their widest, the anterior chambers were approximately 50 mm in diameter. Caudal to the ostia of the anterior chambers, the remainder of the nasopharyngeal duct continued through a tight constriction in the pterygoids that we refer to as the "pterygoid waist" before expanding into a more abbreviated posterior chamber than Louise. As with Louise, the nasal septum in Taj terminated at the start of the pterygoid bullae, leaving both nasal passages confluent for the remainder of their course. We did not observe any defined troughs for the nasopharyngeal duct in Taj like we did in Louise.

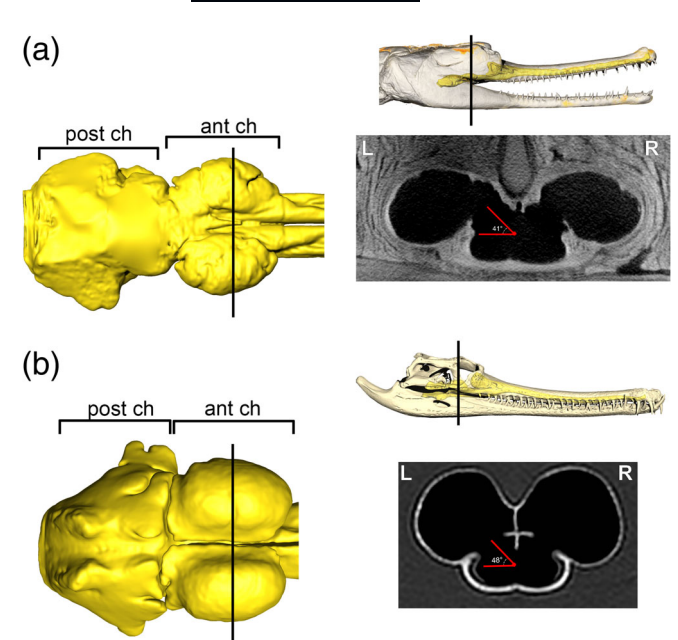
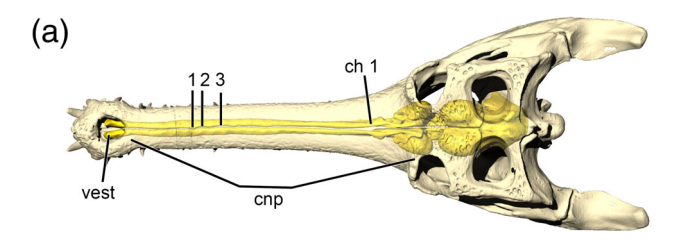


FIGURE 8 Pterygoid bullae in Louise (TNHC 110000, a) and Taj (SA91285, b). CT cross sections taken at approximately the same location in both individuals. Angles represent the mean angle from the center of the air field to the ostium of the anterior chamber. R and L indicate the left and right side of the nasal passage. ant ch, anterior chamber; post ch, posterior chamber

3.6 | Airflow values

Based on our specimens' estimated masses (Table 1), and the flow rate formulae from Farmer (2006) and Farmer and Carrier (2000), our calculations produced a high and low-end flow rate for each gharial (19-24 L/min and. 65-77 L/min). Cross-sectional analyses of the nasal passages at both flow rates indicated that the low-end estimate was more likely to be physiological viable as it produced mostly laminar flow through the majority of the nasal passages. Laminar flow has been shown to be more typical of resting respiration (Craven et al., 2009; Jiang & Zhao, 2010; Lafortuna et al., 2003). In contrast, the highend estimates routinely pushed the air field into turbulent territory (Table 2). Turbulent flow increases internal fluid resistance by the square of velocity (Swift, 1982), requiring more energy to move air through the respiratory system. Adjustments to nasal anatomy and physiology (e.g., increased airway patency and the transition to mouth breathing at high flow rates) indicate that vertebrates avoid moving turbulent air through the respiratory system if possible (Bourke & Witmer, 2016; Churchill et al., 2004; Fregosi & Lansing, 1995; Lafortuna et al., 2003). Using this approach, we opted for the lower flow rate estimate in our gharial specimens with the caveat that our estimates should not be viewed as a ceiling for the restful breathing capacity of gharials, much less their active capacity. Similarly, though our flow rate data serve



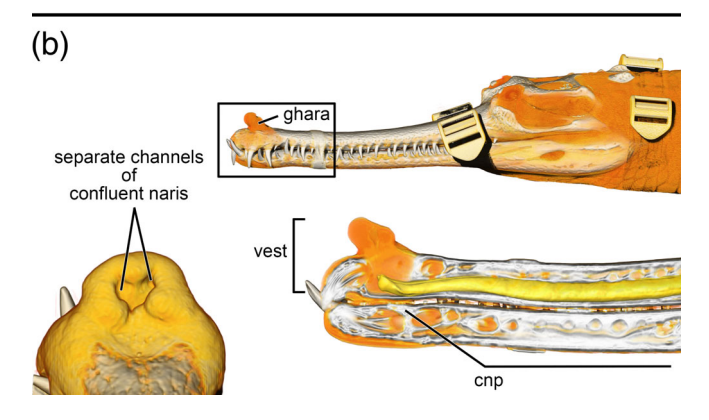


FIGURE 9 Nasal passages of Taj (SA91285). (a) Dorsal view of nasal passage showing the individual waves of the CNP (numbers). (b) Midsagittal view of the nasal vestibule and CNP, with dorsal view of the confluent naris. ch1, primary choana; cnp, cavum nasi proprium; vest, nasal vestibule

as a useful metric for comparison between specimens, the mass estimates used to obtain these values should be viewed with caution. The differences in snout shape and body proportions between alligators and gharials likely limits the ability of broad-snouted-alligator-based respiration equations to accurately capture the respiratory capacity of the much thinner-snouted gharials.

3.7 | Airflow description for Louise (TNHC 110000)

Airflow through the nasal passage was mostly laminar during both phases of respiration. However, the extensive sinuosity observed in the CNP resulted in repeated separation of the air field, producing vortices around the apex, or oxbow of each wave (Figure 10). The region of highest turbulence was observed in the caudal-most bend of both nasal passages (Figure 10b,c). This bend in the nasal passages was the most acute of the bends observed in Louise and resulted in substantial airflow separation as well as extensive compression of the left nasal passage (Figure 10c). Caudal to the final wave of the deviated septum, the air field regained laminarity and continued into the primary choana where a portion of the air field jetted into the olfactory recess. This slower moving air traversed the concha and postconcha dorsally before wrapping ventrally around the conchae and exiting the olfactory recess

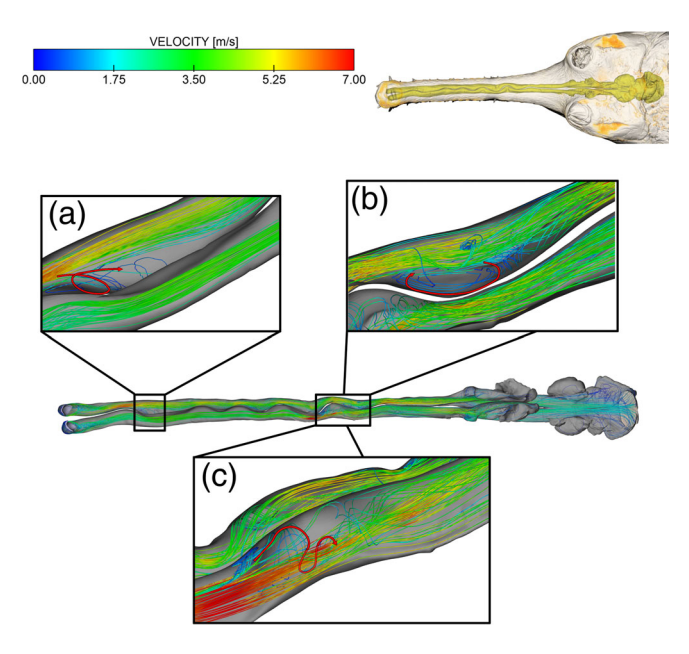


FIGURE 10 Inspiratory airflow through the nasal passage of Louise (TNHC 110000) as represented by 100 pathlines seeded from the nostril. Close up of flow separation at the apex of the first wave (a) and the fifth wave (b) in the right nasal passage. (c) Flow separation in apex of wave in left nasal passage. Arrows added to highlight main flow pattern of interest. Pathlines color-coded for velocity. Artificial nostril inlet omitted for clarity

through a return channel to rejoin the main air field in the nasopharyngeal duct (Figure 11). The air field continued caudally toward the secondary choana. The large ostia for the anterior chambers of the pterygoid bullae in Louise allowed some incident air to enter it from its caudal aspect. Air trapped in the anterior chambers made a shallow counterclockwise traversal through the enlarged structures before rejoining the main air (Figure 12a). The majority of the air field remained centralized to the nasopharyngeal duct, with only small portions of the air field drifting out into the anterior chambers (Figure 12a). The posterior chamber, in contrast, was completely filled with the inspired air field as it made its way toward the secondary choana. The troughs observed for the nasopharyngeal duct, did little to maintain airflow separation. Air streams from the center of the air field emptied directly into the secondary choana, with more peripheral air streams recirculating the posterior chamber before exiting the secondary choana.

Airflow patterns during expiration were similar to inspiration, albeit with air flowing in the opposite direction. A notable change from inspiration was the increase in airflow through the anterior chambers of the pterygoid bullae. Whereas nominal airflow was observed during inspiration, more flow occurred during expiration (Figure 12b). Air entered the anterior chambers from the rostral aspect of the ostia, where it meandered around

the anterior chambers before rejoining the main air field near where it entered (Figure 12b). Air largely bypassed the olfactory recess as it moved into the primary choana (Table 3). As with inspiration, the sinuosity of the nasal passages rostral to the primary choana, produced vortices at the apex of several waves. However, this vortex shedding was less common compared to inspiration.

Comparing pressure distribution across the nasal passages during both phases of respiration, we noticed a substantial pressure disparity between each side of the nasal passages rostral to the primary choana (Figure 13a,c). The right nasal passage showed a steeper pressure gradient than the left at equivalent locations during inspiration (Figure 13a). During expiration, the pressure disparity flipped, and the left side showed the steeper gradient (Figure 13c). This pressure disparity ultimately favored the right nasal passage, moving 12.6% more air through the right side during inspiration and 5.2% more air during expiration (Table 4).

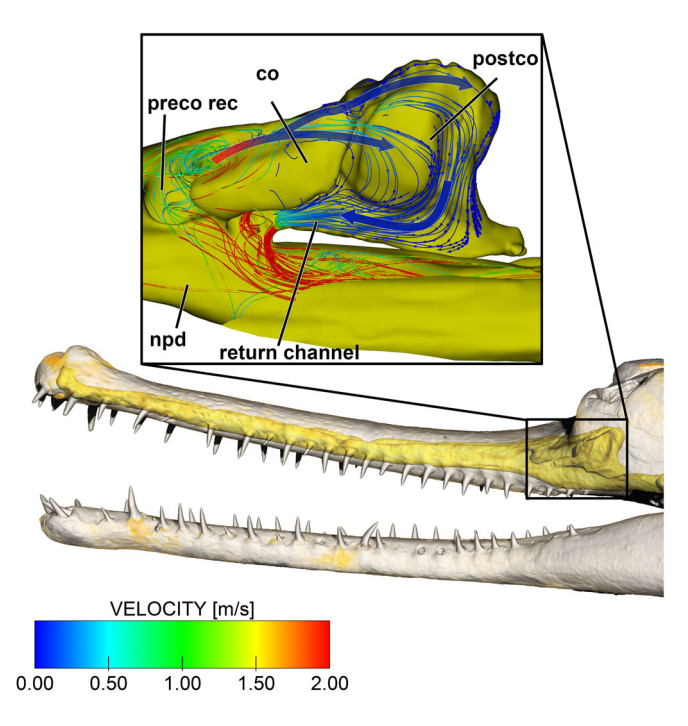


FIGURE 11 Right medial view of the nasal passage and olfactory recess of Louise (TNHC 110000). Olfactory streams shown flowing dorsal to ventral around the conchae. Air streams represented by 100 stream lines seeded from a cross section located at the primary choana. co, concha; npd, nasopharyngeal duct; post co, postconcha; preco rec, preconchal recess

3.8 | Airflow description for Taj (SA91285)

Airflow during inspiration remained laminar throughout the nasal passage with the exception of the trough of the first wave—which produced minor flow separation—and the junction between the primary choana and the olfactory recess where some the air field separated into olfactory and respiratory channels (Figure 14). As with Louise, air streams in the olfactory recess traversed the depth of the recess along the dorsum of the conchae before wrapping around the ventral aspect and forming a return channel that ran ventrally along the recess to rejoin the main air field in the nasopharyngeal duct (Figure 14b). Air inside the nasopharyngeal duct produced some vorticity near the junction with the primary choana, but soon returned to laminarity for the remainder of the nasal passage (Figure 14b). Most of the air field bypassed the anterior chambers of the pterygoid bullae (Figure 12c). Air streams that did enter the ostia of the anterior chambers, made shallow circulations within the chambers before exiting back through the ostia to rejoin the main air field. From here, the entire air field funneled through the pterygoid waist to fill the posterior chamber prior to exiting the secondary choana. Most of the air field took a direct path to the secondary choana with only peripheral parts of the air field extending into the rest of the posterior chamber.

Airflow during expiration remained laminar with no real vorticity observed aside from simulation artifacts near the secondary choana (a consequence of using the secondary choana as a flow source). Unlike Louise, we observed approximately an equivalent amount of air entering the anterior chambers of the pterygoid bullae during expiration as during inspiration (Figure 12d). Expired air entering the anterior chambers traversed a larger proportion of the chambers before exiting the ostia and reentering the main air stream. We observed extremely low flow rate through the olfactory recess during expiration (Table 5), indicating that olfactory flow is largely bypassed during this phase of respiration. From the primary choana, expired air continued rostrally in a mostly straight path to exit the nose at the nostrils. No vorticity was observed in the CNP during expiration.

As with Louise, a pressure differential was observed between the left and right nasal passages during both

TABLE 3 Flow rate (ml/s) through the olfactory recess and NPD of Louise (TNHC 110000)

Phase	Right olfactory recess	Left olfactory recess	Right NPD	Left NPD
Inspiration	3.10	5.19	114.52	107.89
Expiration	0.69	0.93	96.71	76.42

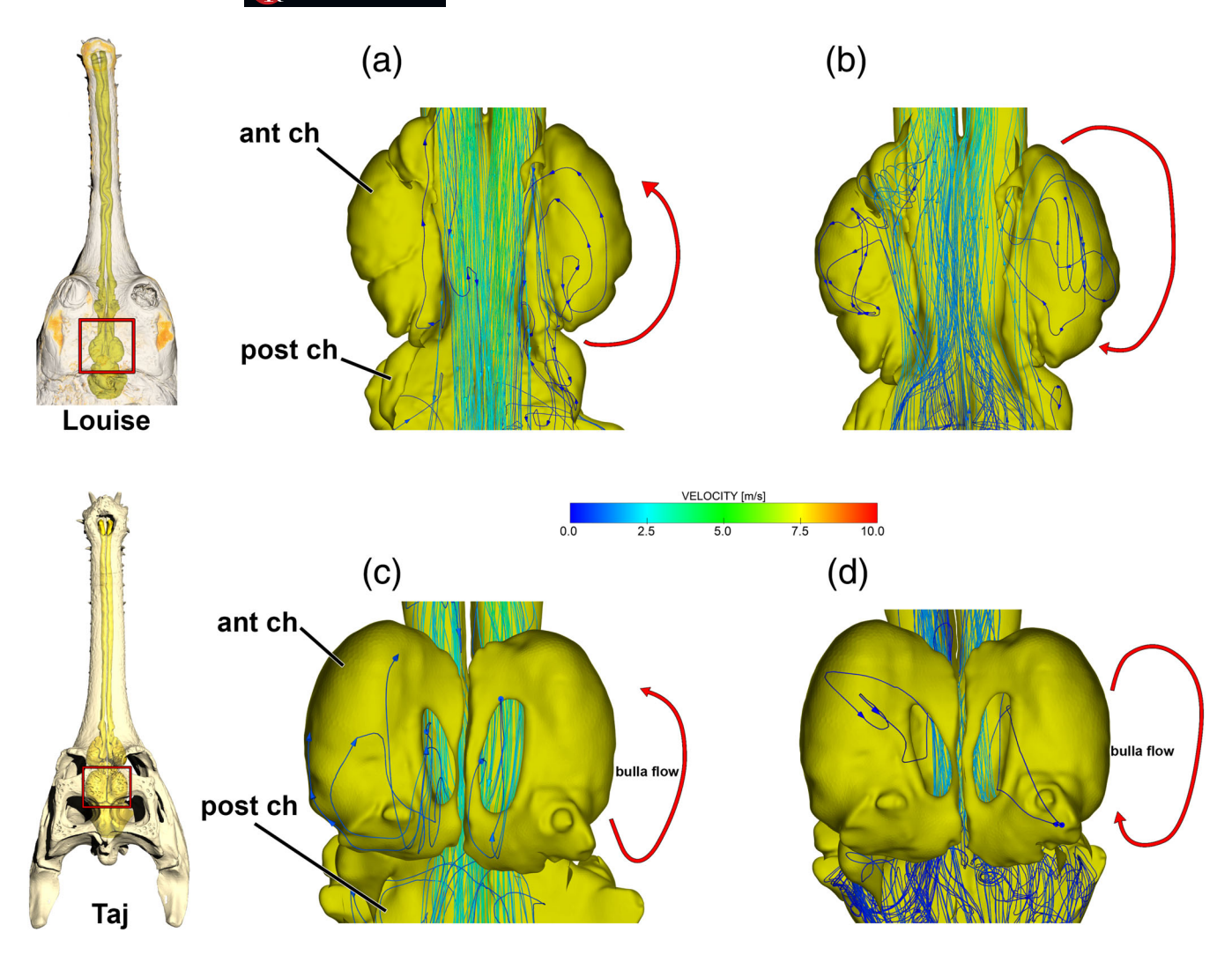


FIGURE 12 Airflow in the pterygoid bullae of Louise (TNHC 110000, a, b) and Taj (SA91285, c, d) during inspiration (a, c) and expiration (b, d). Airflow represented by 100 pathlines seeded from the nostril (inspiration) or choana (expiration). ant ch, anterior chamber; post ch, posterior chamber

phases of respiration (Figure 13b,d). The pressure differential initially favored the right nasal passage during inspiration and later switched to favor the left nasal passage during expiration. Despite a similar pattern to Louise, the pressure differential between both sides of the nasal passage was much smaller (Figure 13b,d). This small pressure differential resulted in an almost equal flow rate between both sides of the nasal passage (Table 4).

3.9 Resistance and wall shear stress

Nasal resistance to airflow was similar for both specimens, with Taj being 5% lower than Louise (Table 6). Wall shear stress values for Louise and Taj showed near identical maxima (2.5 and 2.0 pa, respectively). However, the average wall shear stress was noticeably higher in Louise, with more pockets of high wall shear

stress located at the bends of the deviated septum (Figure 15a,c).

3.10 | Septum width

Nasal septum thickness varied with longitudinal distance rostral to the primary choana (Figures 16a and 17). The septum was thinnest in the gharials compared to the other crocodylians, with *C. johnstoni* coming closest in proportional width (Figure 17b). In the gharials, the nasal septum was thinnest in the region of the rostrum comprised solely of the maxillae (Figure 16a).

4 | DISCUSSION

We were surprised to discover that *Gavialis* has confluent nostrils. All other extant crocodylians maintain separation

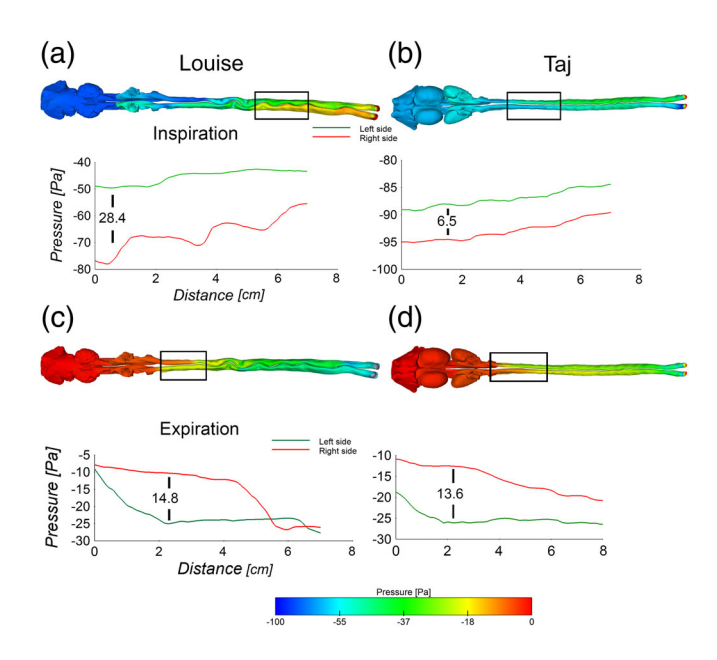


FIGURE 13 Comparison of pressure divergence between left and right nasal passages in Louise (TNHC 110000, a, c) and Taj (SA91285, b, d) during inspiration (a, c) and expiration (b, d). Graphed data represent points taken along lines running proximal to distal within each nasal passage. Artificial nostril inlet omitted for clarity

TABLE 4 Flow rate (ml/s) at primary choana for both nasal passages

	Inspiration		Expiration	
Specimen	Left	Right	Left	Right
Louise	116	149	115	127
Taj	145	157	198	203

of their nostrils. Physiologically, the separation of the nasal passages allows for spatial discrimination of inhaled odors, with even the closely spaced nostrils of humans capable of spatial discrimination within 7° – 10° over a very short period of time (von Békésy, 1964). The presence of a single nostril imposes limits on the ability of the brain to effectively separate olfactory cues in space as air from both sides of the nose will be drawn in and potentially mixed together before funneling into the two nasal passages. This limitation suggests that gharials may have a reduced sense of smell compared to other crocodylians, or at least a reduced capacity to spatially discriminate odors.

Compared to other crocodylians, the nasal septum in *Gavialis* is remarkably thin (Figures 16 and 17). This reduced width is not uniform across the septum but instead shows a tapering in the midline, resulting in an I-beam configuration with the widest parts of the septum along the dorsal and ventral bases. Nasal septum width

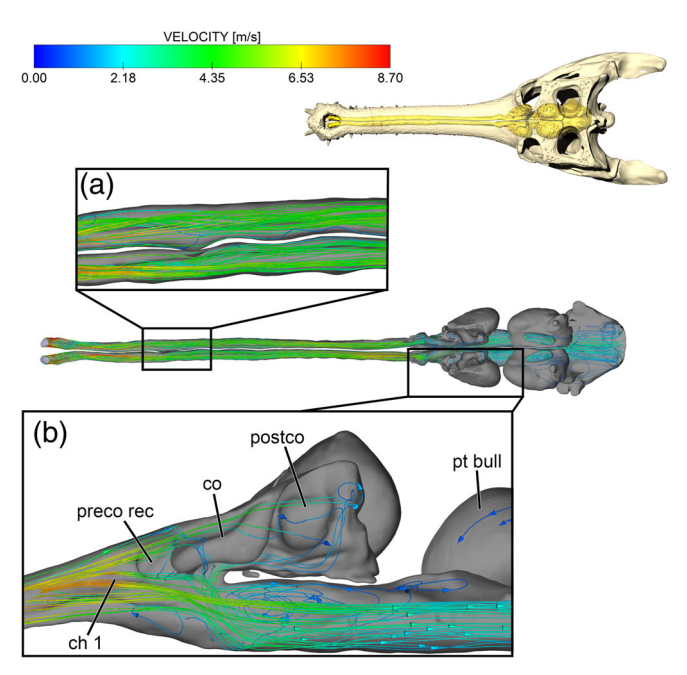


FIGURE 14 Inspiratory airflow through nasal passages of Taj (SA91285). (a) Partial flow separation in the apex of largest wave in CNP. (b) Air field separation into olfactory and respiratory streams at primary choana. Artificial nostril inlet omitted for clarity. ch1, primary choana; co, concha; post co, postconcha; pt bull, pterygoid bulla; preco rec, preconchal recess

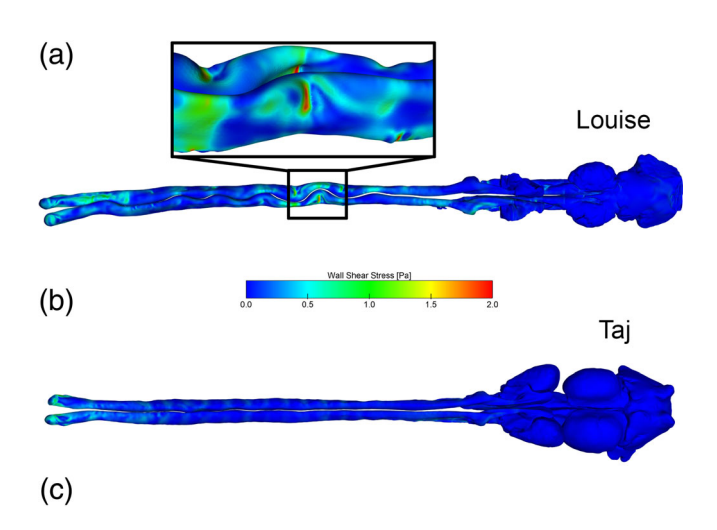
varies longitudinally as well. At the junction of the primary choana and the nasopharyngeal duct, the nasal septum is relatively thick and blends into the interorbital septum caudally. However, rostrally beyond the vomers, the septum thins out considerably (Figure 16a). The vomers provide a solid base for the septal sulcus, resulting in a relatively thick nasal septum wherever the vomers are present. Rostrally past the vomers, the septal sulcus is maintained via a shallow divot formed by the adjoining palatal processes of the maxillae. In some locations along the rostrum, the septal sulcus disappears entirely, and the septum is instead lifted by a raised ridge from the adjoining palatal processes of the maxilla (Figure 16a). As such, in regions of the snout rostral to the vomer, the nasal septum is reliant on the proper suturing of the two parallel maxillae. Tubular compression of the maxillae in Gavialis may explain why this region of the nasal septum is at its thinnest here (Figure 16a). In Louise, the suturing of the palatal processes of the maxillae did not occur uniformly, and the septal ridge routinely swapped positions between maxillae (Figure 18). We suspect that this back and forth of the palatal processes of the maxillae led to the extensively wavy septum observed in this specimen, making this a developmental anomaly somewhat akin to wry nose in horses (Gaughan & DeBowes, 1993). A similar pattern in

TABLE 5 Flow rate (ml/s) through the olfactory recess and NPD of Taj (SA91285)

Phase	Right olfactory recess	Left olfactory recess	Right NPD	Left NPD
Inspiration	0.84	5.34	128.25	80.26
Expiration	0.43	0.80	173.55	117.09

TABLE 6 Pressure, flow rate, and resistance for the nasal passages during inspiration

Specimen	Mean pressure at choana (pa)	Flow rate (ml/s)	Resistance (pa·s/ml
Louise	-65.26	313	0.21
Taj	-82.70	407	0.20



specimen	mean (Pa)	max (Pa)
Louise	0.13	2.54
Taj	0.05	2.04

FIGURE 15 Wall shear stress distribution along the nasal passages of Louise (TNHC 110000, a) and Taj (SA91285, b). Mean and maximum wall shear stress between each specimen (c). Inset: Close up of maximum shear stress along the fifth wave of the deviated septum. Artificial nostril inlet omitted for clarity

nasal septum shape and width reduction can be seen in alligatorids and crocodylids (Figure 16b). However, in these taxa, the divot in the adjoining maxillae is deeper and maxillary length is shorter, leading to straight septum for the entire length of the nasal passage. Of the specimens we surveyed, only the *C. johnstoni* and the juvenile *C. porosus* had similarly thin nasal septa, though both of these were true only in an absolute sense. Proportionally, the nasal septum in the crocodylids was still thicker than in *Gavialis* (Figure 17b). Of the two crocodylids, *C. johnstoni* is the closest in rostrum shape to *Gavialis* (Figure 6). Both longirostrine crocodylians had tube-shaped nasal passages in the rostrum, as

opposed to the wider, flatter nasal passages of our brevirostrine taxa (e.g., Figures 6 and 16b). Widening the rostrum offers more room for the corresponding nasal passages and allows for the maintenance of a thicker nasal septum. For longirostrine taxa, space within the tubular rostrum is at a premium. The smaller space for the nasal passages, coupled with the competing spatial needs of replacement teeth (Figures 16a and 18) necessitates a thinner nasal septum to provide enough air for normal respiration without an excessive increase in respiratory resistance.

To the best of our knowledge, this represents the first instance of a deviated septum presenting as a wavy structure in an amniote. Septal deviations more typically present as a singular incursion into one nasal passage (Eren et al., 2014; Peralta et al., 2017) rather than the alternating compression of both nasal passages as we observed here (Figure 18). Although nasal septum deviation was witnessed in both Taj and Louise, the degree of septal deviation was much larger in Louise and had distinct physiological ramifications. Septal deviation in Louise produced an uneven pressure distribution across the nasal passages during both phases of respiration, resulting in uneven flow patterns (Figure 13a,c; Table 4). The alternating compression of each side of the nasal passage in Louise resulted in slightly higher respiratory resistance in this specimen as opposed to Taj (Table 6). This was surprising given the 30% higher flow rate for Taj. Despite Taj respiring a larger volume of air over a longer distance through the rostrum (51 mm, or 12% longer than Louise), this specimen showed lower resistance than Louise. This increased resistance would have increased the cost of breathing for Louise. To achieve the same flow rate as Taj, Louise would need to steepen its pressure gradient by 2.6% or 2.2 Pa. Though this modest change is well within the energetic scope of the animal, it remains noteworthy as Louise was a smaller animal with an essentially identical nasal anatomy and all of these values were for resting respiration. Increased oxygen demand

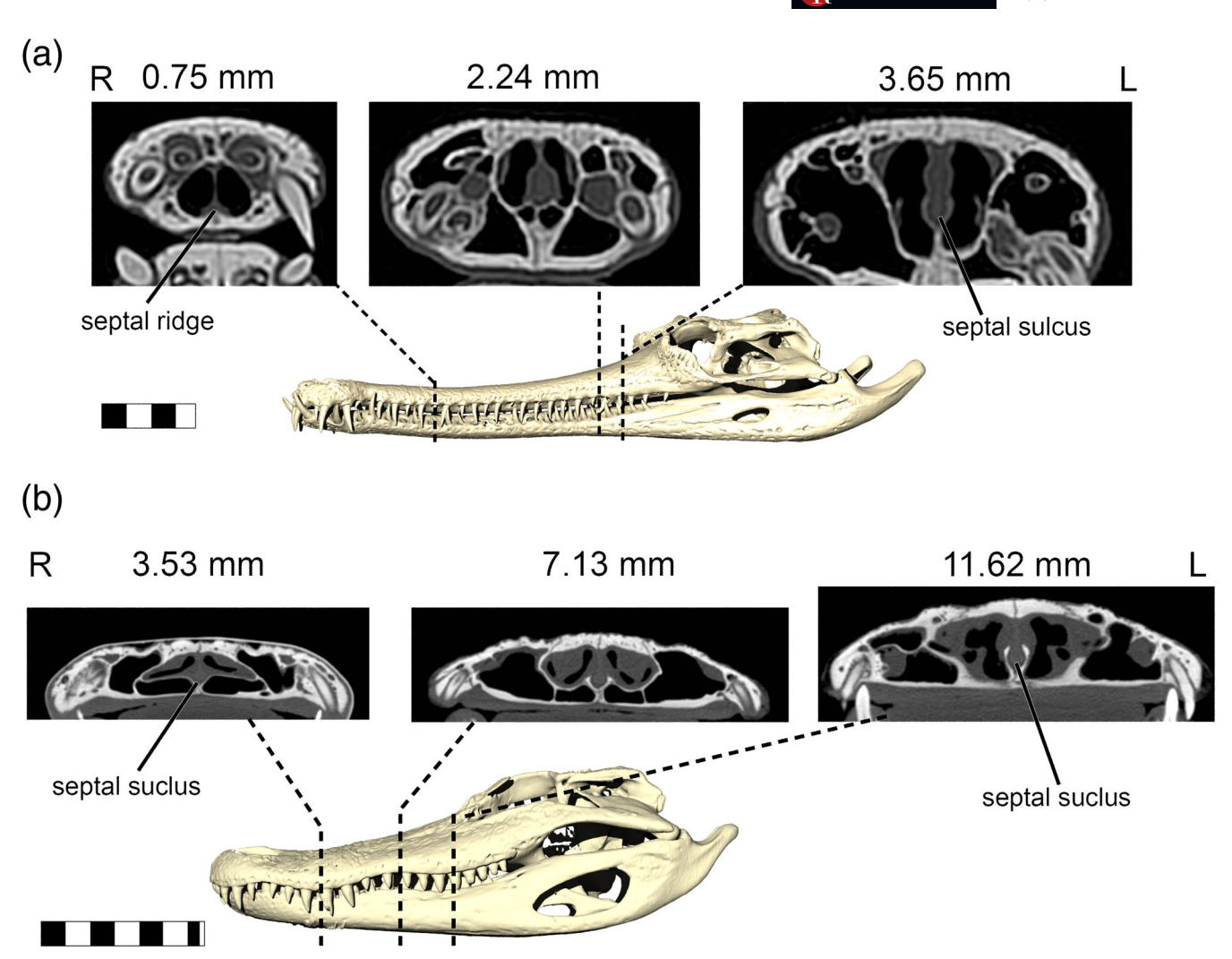
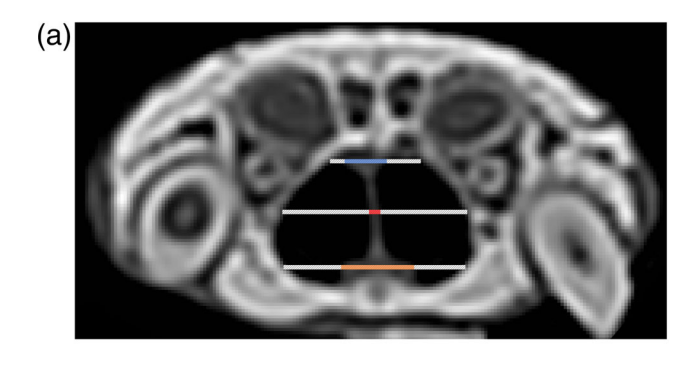


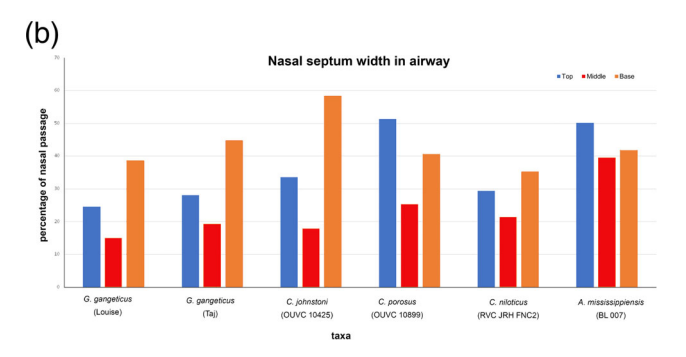
FIGURE 16 Cross sections of the nasal cavity taken at the primary choana, rostral end of vomer, and maxilla-only region of *Gavialis* (a, SA91285) and *Alligator* (b, BL-007). Scale bar = 10 cm. Measurements represent the width of the nasal septum at its midline. R and L indicate right and left orientation of CT images

from activity would only increase this discrepancy. The effect of this increased resistance is best seen when comparing the wall shear stress along the nasal passage of both specimens (Figure 15). Maximum wall shear stress values were near identical between the two specimens, but the distribution of that shear stress was much greater in Louise (Figure 15). Wall shear stress acts as gauge for flow resistance by endothelial and epithelial cells (Ku, 1997). High wall shear stresses act as a stimulus for these cells to act in a manner to reduce resistance, such as blood vessel widening and arborization (Ando & Yamamoto, 2009; Vogel, 1994). In the nasal passages, high wall shear stress has been associated with excess mucous secretion, cilia damage, keratinization, and spontaneous epistaxis (Bailie et al., 2009; Elad et al., 2006). The peak wall shear stress values recorded in our gharials (2.0-2.5 Pa) are higher than similar studies of rat and human nasal passages (0.755-1.0 Pa; Elad et al., 2006;

Shang et al., 2017) and are within the preferred maintenance range of arteries (Ku, 1997). Peak wall shear stress values corresponded to areas of high velocity flow and turbulent eddies. These regions were limited largely to the vestibule-CNP junction in Taj but included many of the sinuous waves in the deviated septum of Louise (Figure 16). These peak wall shear stress areas in Louise may have produced localized damage to the mucosa and/or accelerated mucous secretion in the nose of this individual to compensate for the relatively high shear rate. The presence of a many high wall shear stress values in Louise and the $2.6\times$ higher average wall shear stress compared to the larger Taj lend support to the hypothesis that this specimen's uniquely deviated septum did impair nasal passage function.

Airflow in the olfactory recess of both gharial specimens was unidirectional during inspiration and largely stagnant during expiration (Tables 3 and 5), as expected





of the nasal passages of gharials and representative crocodylians.

(a) Sample measurement of nasal septum width taken from the top, midline, and base (opaque lines). Measurements are compared to total available nasal passage width from those same locations (hatched lines). (b) Graph of nasal septum proportions taken along the length of the nasal passage, rostral to the primary choana in both gharial specimens, and compared to similar measurements from other crocodylian species

of a macrosmatic animal (Craven et al., 2010). We did observe remarkably low olfactory flow in the right olfactory recess of Taj during inspiration, with the left olfactory recess moving $6\times$ the volume of air through it. We saw no sign of nasal septum deviation in this region, but we did observe differences in preconcha thickness between the left and right nasal passage near the primary choana. Crocodylians have a large vascular plexus in this region (Porter et al., 2016) that can potentially affect the thickness of the preconcha mucosa and could explain the slight differences in mucosa thickness observed here.

That both gharial specimens exhibited some degree of septal deviation was surprising and suggests that longirostry in Crocodylia may leave these more specialized species susceptible to septal deviations that can lead to increased costs of breathing and possibly limited olfactory abilities. Future surveys of the nasal passages of *Tomistoma schlegeli* and *Crocodylus intermedius* (extant longirostrine crocodylians that were unavailable for study at this time) would greatly aid to this hypothesis. In the past, the presence of a long, thin rostrum was not limited

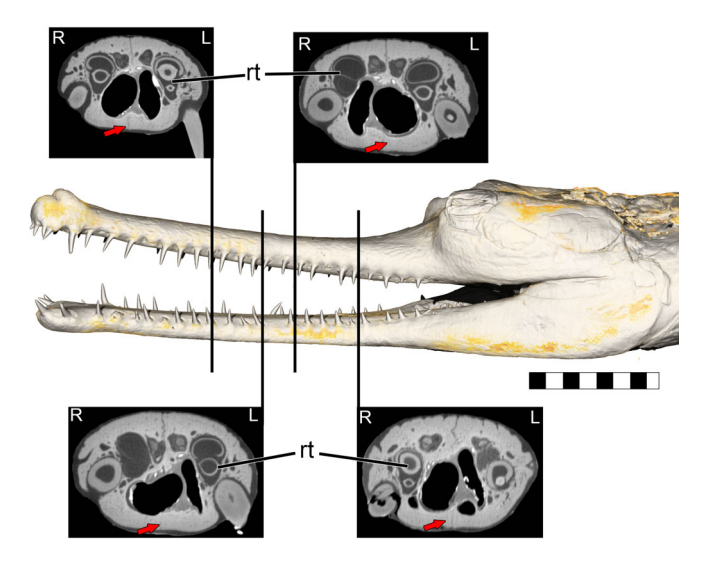
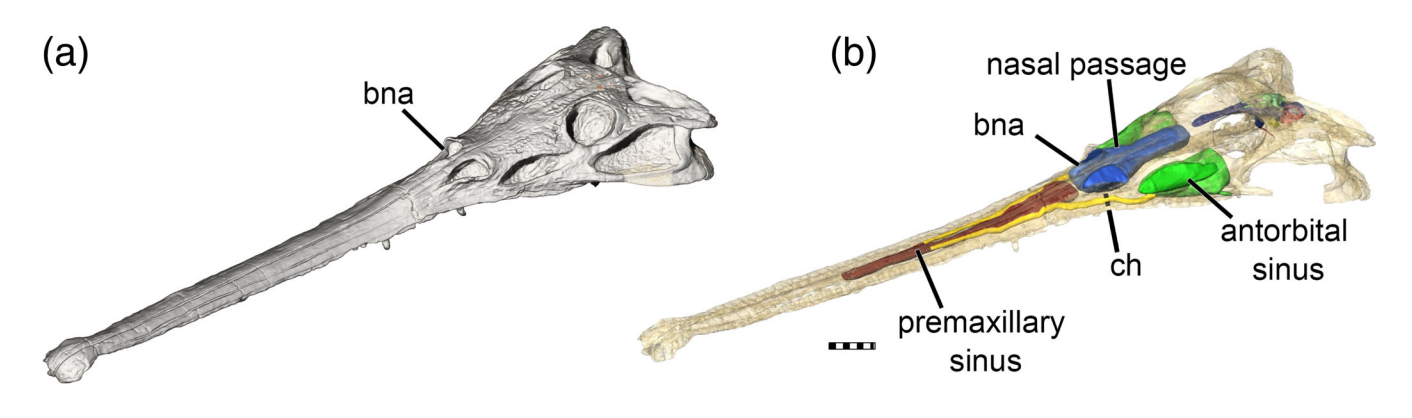


FIGURE 18 Sample CT images along the rostrum of Louise (TNHC 110000), showcasing the extent of the nasal septum deviation. Arrows show the location of the palatal process suture. Scale bar = 10 cm. R and L indicate right and left orientation of CT images. RT, replacement tooth

to Crocodylia, or Crocodylomorpha. Various extinct reptile groups explored this morphospace and may have been susceptible to similar nasal passage abnormalities (Figure 19). Phytosaurs—sister group to Archosaurs (Nesbitt, 2011)—had remarkably crocodylian-like body plans including elongated rostra. However, unlike crocodylians, this group moved their nasal passages caudally, placing them close to (and sometimes above) the orbits (Lautenschlager & Butler, 2016). The elongated snout did retain an air space (likely a paranasal sinus) but would not have housed the nasal passages and thus would not have been susceptible to this type of nasal passage pathology (Figure 19a,b). Among dinosaurs, spinosaurids showed remarkable convergence in skull shape with longirostrine crocodylians, making them potential candidates for septal deviation. Looking at the skulls of spinosaurids, we find evidence of retraction of the bony nasal aperture Dal Sasso et al., 2005; Figure 19c). As this is the entrance into the skull for the airway, retraction of the bony nasal aperture effectively reduced the length of the nasal septum in this group to just the caudal-most region of the nasal passage (olfactory recess and nasopharyngeal duct). In contrast to these two groups, members of Choristodera may be the most analogous to extant longirostrine crocodylians (Figure 19d). This enigmatic group of reptiles includes many species that took on a decidedly gharial-like bauplan complete with skulls that housed very elongated nasal passages (Dudgeon et al., 2020). Given this similarity snout shape and nasal passage placement, choristoderans may have been particularly susceptible to this type of nasal pathology. This



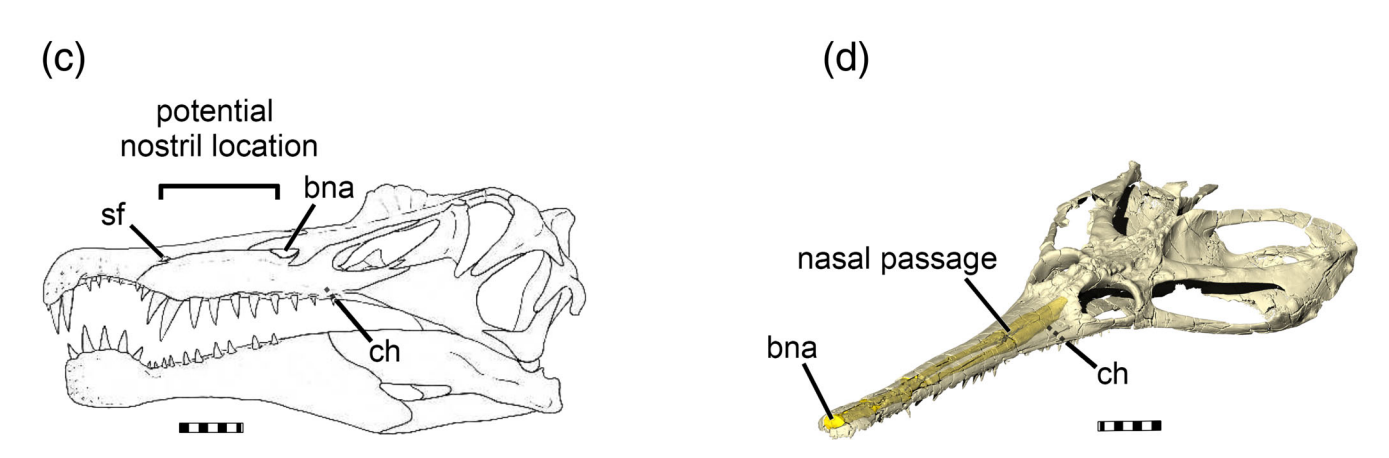


FIGURE 19 Selected reptilian taxa that converged on a longirostrine morphology. (a) The phytosaur, *Ebrachosuchus neukami* with segmented airway and paranasal sinuses (b). (c) The spinosaurid, *Spinosaurus aegyptiacus*. (d) The choristoderan, *Champsosaurus lindoei*. (a) and (b): adapted from Lautenschlager and Butler (2016). (c): adapted from Dal Sasso et al. (2005). (d): based on data originally published by Dudgeon et al. (2020). bna, bony nasal aperture; ch, choana; sf, subnarial foramen

could be assessed by following suture lines along the palatal side of the nasal passages in well-preserved skulls.

4.1 | Pterygoid bulla

All of our gharial specimens had well-developed pterygoid bullae (Figures 5 and 8). This was unexpected as pterygoid bullae have been hypothesized to be sexually dimorphic structures associated with mature males (Geoffroy, 1825; Hone et al., 2020; Kälin, 1933). Taj was a mature adult male and was expected to have pterygoid bullae along with at least a partially developed ghara. In contrast, Louise represented an old, mature female. This indicates that the pterygoid bulla is not restricted to males and casts doubt on the use of this anatomical structure for determining sex in gharial skulls. That said, the morphology of the pterygoid bulla in both specimens was noticeably different (Figures 8 and 20). The pterygoid

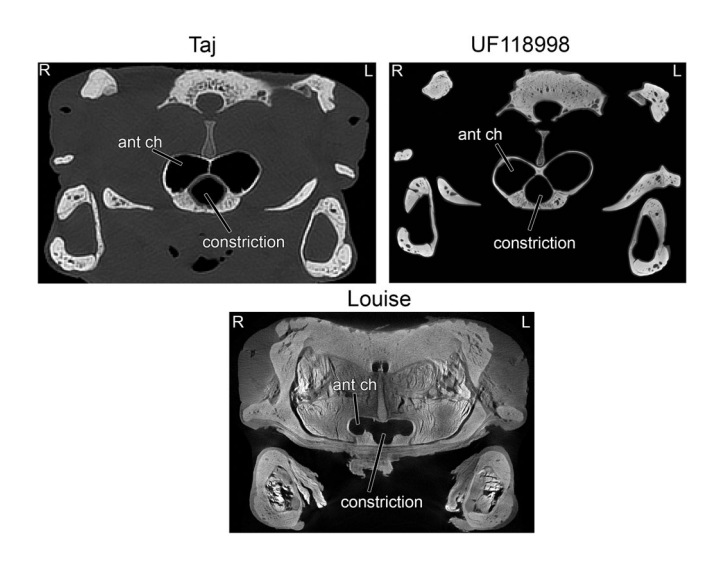


FIGURE 20 Axial cross sections comparing constrictions (pterygoid waists) between our three gharial specimens. R and L indicate right and left orientation of CT images. ant ch, anterior chamber

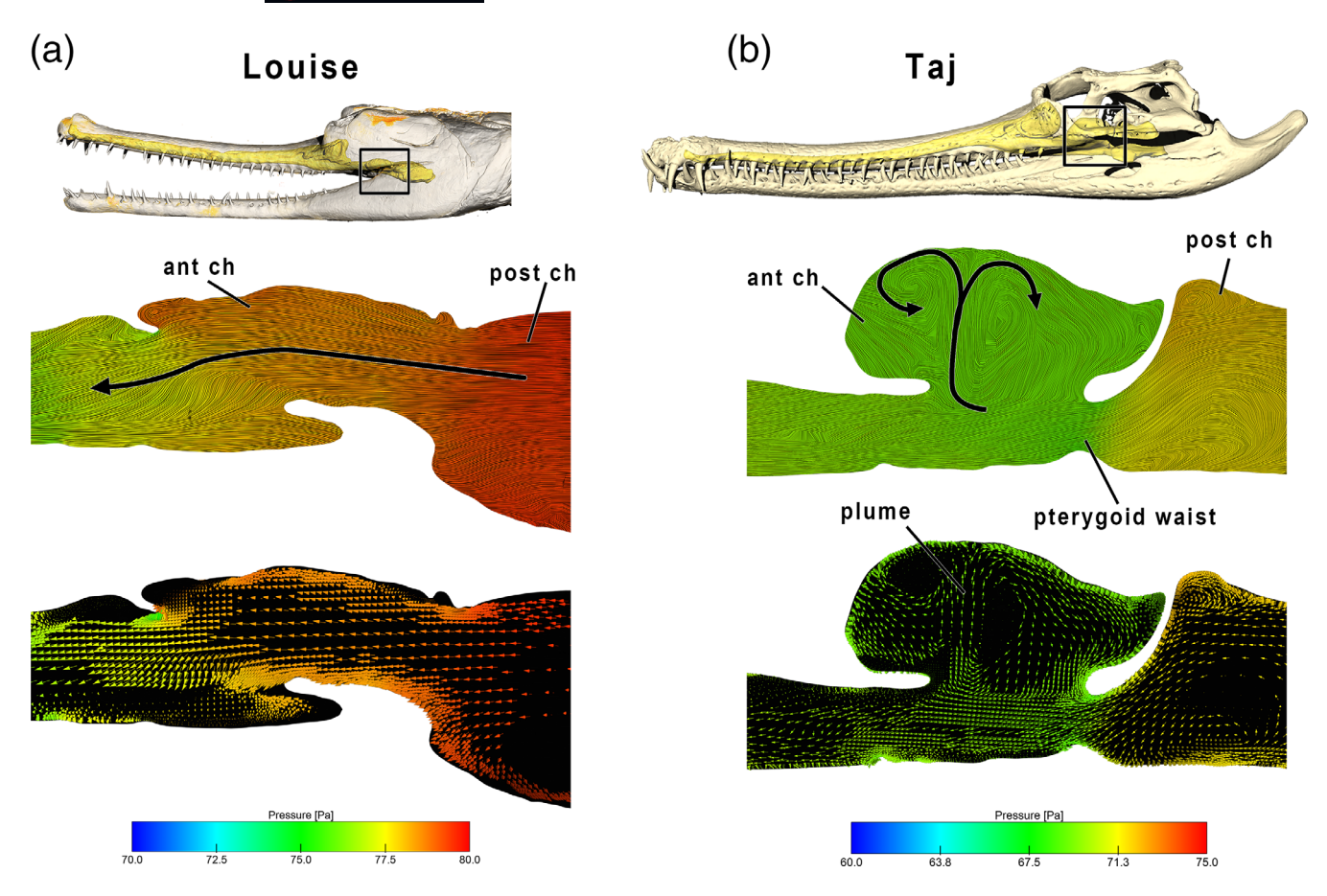


FIGURE 21 Sagittal sections midway through the ostium of the right anterior chamber of the pterygoid bulla of Taj (SA91285, a) and Louise (TNHC 110000, b) during expiration. Cross sections are color coded for pressure. Bottom cross sections feature vector arrows showing the flow field at this location. Note the plume of air jetting into the anterior chamber of Taj. ant ch, anterior chamber; post ch, posterior chamber

bullae in Taj formed almost immediately distal to the olfactory recess and consisted of strongly rounded anterior chambers with well-defined ostia and a constricted pterygoid waist between the anterior and posterior chambers (Figures 8 and 20). In contrast, Louise's pterygoid bullae formed further caudally from the olfactory recess. The anterior chambers were wider, but less rounded and more oblong with poorly defined ostia and no pterygoid waist separating the anterior and posterior chambers (Figure 8a). UF118998 was a dried skull specimen that also preserved pterygoid bullae. These bullae were shaped similar to the bullae in Taj (Figure 20). This specimen also contained a shallow narial fossa as an attachment site for a ghara (Hone et al., 2020), indicating that UF118998 was likely a male. Though pterygoid bullae do not appear to conform well to a binary presence/absence categorization of sex (Hone et al., 2020), the shape of the bullae and their connection to the nasopharyngeal duct may still be dimorphic. The caveat here being the limited dataset for our interpretation, consisting of two wet specimens and one dried skull of unconfirmed sex.

In reviewing our CFD analysis, we observed that the bullae received moderate ventilation during both phases of respiration (Figure 12). Notably, the nasal passages became confluent at the bullae for both Taj and Louise. This turned the bilateral pterygoid bullae into a singular structure. Gavialis appears to merge its nasal passages from both the rostral and caudal ends, which may be important for sound production. The bulla, like the ghara, has been hypothesized to function in sound production based on its direct connection to the nasal passages (Hone et al., 2020; Martin & Bellairs, 1977). The morphological difference between the pterygoid bullae in Taj and Louise, produced different pressure profiles and flow patterns. These flow patterns became more prominent when the expiration model incorporated positive pressure from the choana (80 Pa, Figure 21). In Taj, the pterygoid waist between the anterior and posterior chambers produced a Bernoulli effect (Vogel, 1994), funneling relatively high velocity air from the posterior chamber into the anterior chamber, and jetting some of that air into a plume around the anterior chambers (Figure 21b).

Louise, in contrast, showed no sign of a Bernoulli effect. Instead, air flowed through both chambers of the pterygoid bullae with little impedance (Figure 21a), forming only shallow, horizontal circulation patterns within the oblong anterior chambers. Gharials are able to produce a unique "pop" sound through closed jaws (Jailabdeen et al., 2019). These pops are short in duration (0.013-0.036 s) and repeatable up to at least three times in succession. We suspect that the pterygoid bullae are responsible for these pops by incorporating the Bernoulli effect into the physical structure of the pterygoid bulla via the pterygoid waist. This would make gharial "pops" similar to the bilabial plosive sounds produced in human speech (Pelorson et al., 1997). Our study was limited to simulating resting respiration, which is unlikely to produce the pressure waves necessary to accurately simulate this type of sound production. Yet, even at these relatively low flow rates, the Bernoulli effect was readily observable (Figure 21b).

5 | CONCLUSION

We described the nasal anatomy and respiratory airflow patterns in the nasal passages of the Indian gharial. We have discovered that gharial nasal passages are fused at their rostral and caudal ends. This fusion may be important for sound production in the unique anatomical structures of the gharial nose, the ghara, and pterygoid bulla. The sinuous septal deviation in the female gharial, Louise, produced turbulent eddies within the rostrum, increasing nasal resistance and imparting greater wall shear stress across the nasal passage during inspiration. Septal deviations were observed in both Louise and the large male, Taj. These deviated nasal septa occurred rostral to the termination of the vomers where septum stability is maintained by proper suturing of the palatal processes of the maxilla. Our data suggest that gharials and other longirostrine crocodylians may be particularly vulnerable to septal deviations, which can adversely affect their respiratory physiology. Lastly, we found evidence that the pterygoid bulla can be found in both sexes, though the morphology of the bulla may still be sexually dimorphic. The presence of a pterygoid waist in males produces a Bernoulli effect on expired air that may be responsible for the distinct "pop" sounds produced by competing males gharials.

ACKNOWLEDGMENTS

The authors would like to graciously thank the editors for inviting them to contribute to this special issue. They would also like to thank the Holliday Lab members for granting access to TNHC 110000 and M. Colbert for

scanning the specimen, K. Vliet for access to the St. Augustine specimen and information on gharial acoustics, the WitmerLab, and Hutchinson Lab for providing their data as open source on the websites Morphosource, Data Dryad, and CrocBase, and lastly, reviewers for their helpful critique and suggestions for this manuscript.

AUTHOR CONTRIBUTIONS

Jason Bourke: Conceptualization (lead); data curation (lead); formal analysis (lead); investigation (equal); methodology (equal); project administration (lead); resources (equal); software (lead); supervision (lead); validation (lead); visualization (equal); writing – original draft (lead); writing – review and editing (equal). Nicole Fontenot: Conceptualization (supporting); investigation (equal); methodology (equal); visualization (supporting); writing – review and editing (supporting). Casey Holliday: Conceptualization (supporting); resources (equal).

ORCID

Jason M. Bourke https://orcid.org/0000-0002-6966-8020 Casey Holliday https://orcid.org/0000-0001-8210-8434

REFERENCES

- Ando, J., & Yamamoto, K. (2009). Vascular mechanobiology endothelial cell responses to fluid shear stress. *Circulation Journal*, 73(11), 1983–1992.
- Bailie, N., Hanna, B., Watterson, J., & Gallagher, G. (2009). A Model of Airflow in the Nasal Cavities: Implications for Nasal Air Conditioning and Epistaxis. *American Journal of Rhinology* & Allergy, 23, 244–249.
- Bass, K., Boc, S., Hindle, M., Dodson, K., & Longest, W. (2019). High-efficiency nose-to-lung aerosol delivery in an infant: Development of a validated computational fluid dynamics method. *Journal of Aerosol Medicine and Pulmonary Drug Delivery*, 32(3), 132–148.
- Bourke, J. M., Porter, W. R., Ridgely, R. C., Lyson, T. R., Schachner, E. R., Bell, P. R., & Witmer, L. M. (2014). Breathing life into dinosaurs: Tackling challenges of soft-tissue restoration and nasal airflow in extinct species. *The Anatomical Record*, 297, 2148–2186.
- Bourke, J. M., Porter, W. R., & Witmer, L. M. (2018). Convoluted nasal passages function as efficient heat exchangers in ankylosaurs (Dinosauria: Ornithischia: Thyreophora). *PLoS One*, *13* (12), e0207381.
- Bourke, J. M., & Witmer, L. M. (2016). Nasal conchae function as aerodynamic baffles: Experimental computational fluid dynamic analysis in a Turkey nose (Aves: Galliformes). *Respiratory Physiology & Neurobiology*, 234, 32–46.
- Chen, X. B. B. E., Lee, P. H., Chong, V. F. H., & Wang, D. Y. (2009). Assessment of septal deviation effects on nasal air flow: A computational fluid dynamics model. *Laryngoscope*, 119, 1730–1736.
- Churchill, S. E., Shackelford, L. L., Georgi, N., & Black, M. T. (2004). Morphological variation and airflow dynamics in the human nose. *American Journal of Human Biology*, 16, 625–638.

- Copray, J. C. V. M. (1986). Growth of the nasal septal cartilage of the rat in vitro. Journal of Anatomy, 144, 99–111.
- Craven, B. A., Paterson, E. G., & Settles, G. S. (2010). The fluid dynamics of canine olfaction: unique nasal airflow patterns as an explanation of macrosmia. *Journal of the Royal Society Interface*, 7, 933–943.
- Craven, B. A., Patterson, E. G., Settles, G. S., & Lawson, M. J. (2009). Development and verification of a high-fidelity computational fluid dynamics models of canine nasal airflow. *Journal of Biomechanical Engineering*, 131, 091002.
- Dal Sasso, C., Maganuco, S., Buffetaut, E., & Mendez, M. A. (2005). New information on the skull of the enigmatic theropod Spinosaurus, with remarks on its size and affinities. Journal of Vertebrate Paleontology, 25(4), 888–896.
- Dinets, V. (2013). Long-distance signaling in Crocodylia. *Copeia*, 2013(3), 517–526.
- Dudgeon, T. W., Maddin, H. C., Evans, D. C., & Mallon, J. C. (2020). The internal cranial anatomy of *Champsosaurus* (Choristodera: Champsosauridae): Implications for neurosensory function. *Scientific Reports*, 10, 7122.
- Elad, D., Naftali, S., Rosenfeld, M., & Wolf, M. (2006). Physical stresses at the air-wall interface of the human nasal cavity during breathing. *Journal of Applied Physiology*, 100(3), 1003–1010.
- Eren, S. B., Tugrul, S., Dogan, R., Ozucer, B., & Ozturan, O. (2014).
 Objective and subjective evaluation of operation success in patients with nasal septal deviation based on septum type.
 American Journal of Rhinology & Allergy, 28(4), e158–e162.
- Erickson, G. M., Gignac, P. M., Steppan, S. J., Lappin, A. K., Vliet, K. A., Brueggen, J. D., Inouye, B. D., Kledzik, D., & Webb, G. J. W. (2012). Insights into the ecology and evolutionary success of crocodilians revealed through bite-force and tooth-pressure experimentation. *PLoS One*, 7(3), e31781.
- Farmer, C. G. (2006). On the origin of avian air sacs. Respiratory Physiology & Neurobiology, 154, 89–106.
- Farmer, C. G., & Carrier, D. R. (2000). Ventilation and gas exchange during treadmill locomotion in the American alligator (Alligator mississippiensis). The Journal of Experimental Biology, 203, 1671–1678.
- Fregosi, R. F., & Lansing, R. W. (1995). Neural drive to nasal dilator muscles: Influence of exercise intensity and oronasal flow partitioning. *Journal of Applied Physiology*, 79(4), 1330–1337.
- Gaughan, E. M., & DeBowes, R. M. (1993). Congenital diseases of the equine head. *Veterinary Clinics of North America: Equine Practice*, 9(1), 93–110.
- Geoffroy, S. H. (1825). Recherches sur l'organisation des gavials. Mémoires du Muséum National d'Histoire Naturelle, 12, 97–155.
- Gignac, P. M., Kley, N. J., Clarke, J. A., Colbert, M. W., Morhardt, A. C., Cerio, D., Cost, I. N., Cox, P. G., Daza, J. D., Early, C. M., Echols, M. S., Henkelman, R. M., Nerdina, A. M., Holliday, C. M., Li, Z., Mahlow, K., Merchant, S., Muller, J., ... Witmer, L. M. (2016). Diffusible iodine-based contrastenhanced computed tomography (diceCT): An emerging tool for rapid, high-resolution, 3-D imaging of metazoan soft tissues. *Journal of Anatomy*, 228(6), 889–909.
- Grigg, G., & Kirshner, D. (2015). Biology and evolution of Crocodylians. Cornell University Press.
- Hone, D., Mallon, J. C., Hennessey, P., & Witmer, L. M. (2020). Ontogeny of a sexually selected structure in an extant archosaur *Gavialis gangeticus* (Pseudosuchia: Crocodylia) with implications for sexual dimorphism in dinosaurs. *PeerJ*, 8, e9134.

- Jailabdeen, A., Lang, J. W., Singh, R. K., & Archunan, G. (2019). Gharial communication: Acoustic signaling via "pops". Proceedings, 13th Western Pacific Acoustics Conference, 11-15 November, New Delhi India, 1-6.
- Jiang, J., & Zhao, K. (2010). Airflow and nanoparticle deposition in rat nose under various breathing and sniffing conditions. *Journal of Aerosol Science*, 41(11), 1030–1043.
- Kälin, J. A. (1933). Beitrage zur vergleichenden Osteologie des Crocodilidenschadels. Zoologische Jahrbücher, 57, 535–714.
- Khadka, B. B., & Bashyal, A. (2019). Growth rate of captive Gharials
 Gavialis gangeticus (Gmelin, 1789) (Reptilia: Crocodylia:
 Gavialidae) in Chitwan National Park. Nepal. Journal of Threatened Taxa, 11(15), 14998–15003.
- Klenner, S., Witzel, U., Paris, F., & Distler, C. (2016). Structure and function of the septum nasi and the underlying tension chord in crocodylians. *Journal of Anatomy*, 228(1), 113–124.
- Ku, D. N. (1997). Blood flow in arteries. Annual Review of Fluid Mechanics, 29, 399–434.
- Lafortuna, C. L., Saibene, F., Albertini, M., & Clement, M. G. (2003). The regulation of respiratory resistance in exercising horses. *European Journal of Applied Physiology*, 90, 396–404.
- Lautenschlager, S., & Butler, R. J. (2016). Neural and endocranial anatomy of Triassic phytosaurian reptiles and convergence with fossil and modern crocodylians. *PeerJ*, 4, e2251.
- Li, C., Jiang, J., Dong, H., & Zhao, K. (2017). Computational modeling and validation of human nasal airflow under various breathing conditions. *Journal of Biomechanics*, 64, 59–68.
- Liu, Y., Matida, E. A., Gu, J., & Johnson, M. R. (2007). Numerical simulation of aerosol deposition in a 3-D human nasal cavity using RANS, RANS/EIM, and LES. *Journal of Aerosol Science*, 38, 383-700.
- Loudon, C., & Tordesillas, A. (1998). The use of the dimensionless Womersley number to characterize the unsteady nature of internal flow. *Journal of Theoretical Biology*, 191, 63–78.
- Martin, B. G. H., & Bellairs, A. A. (1977). The narial excrescence and pterygoid bulla of the gharial, *Gavialis gangeticus* (Crocodilia). *Journal of Zoology*, *182*, 541–558.
- Maskey TM 1989. Movement and survival of captive-reared gharial *Gavialis gangeticus* in the Narayani river, Nepal (PhD thesis) University of Florida, Gainesville, FL.
- McHenry, C. R., Clausen, P. D., Daniel, W. J. T., Meers, M. B., & Pendharkar, A. (2006). Biomechanics of the rostrum in crocodilians: A comparative analysis using finite-element modeling. *Anatomical Record Part A*, 288A, 827–249.
- Moss, M. L. (1976). The role of the nasal septal cartilage in midfacial growth. In *Factors affecting the growth of the midface*. Center for Human Growth and Development, The University of Michigan.
- Mozell, M. M., & Jadodowicz, M. (1973). Chromatographic separation of odorants by the nose: Retention times measured across in vivo olfactory mucosa. *Science*, 181(4106), 1247–1249.
- Nesbitt, S. J. (2011). The early evolution of archosaurs: Relationships and the origin of major clades. *Bulletin of the American Museum of Natural History*, 352, 1–292.
- Parsons, T. S. (1970). The nose and Jacobson's organ. In C. Gans & T. S. Parsons (Eds.), *Biology of the Reptilia* (Vol. 2, pp. 99–191). Academic Press.
- Pelorson, X., Hofmans, G. C. J., Ranucci, M., & Bosch, R. C. M. (1997). On the fluid mechanics of bilabial plosives. Speech Communication, 22(2-3), 155–172.

- Peralta, S., Fiani, N., Kan-Rohrer, K. H., & Verstraete, F. J. (2017). Morphological evaluation of clefts of the lip, palate, or both in dogs. *American Journal of Veterinary Research*, 78(8), 926–933.
- Pierce, S. E., Angielczyk, K. D., & Rayfield, E. J. (2008). Patterns of morphospace occupation and mechanical performance in extant crocodilian skulls: A combined geometric morphometric and finite element modeling approach. *Journal of Morphology*, 269, 840–864.
- Porter, W. R., Sedlmayr, J. C., & Witmer, L. M. (2016). Vascular patterns in the heads of crocodilians: Blood vessels and sites of thermal exchange. *Journal of Anatomy*, 229, 800–824.
- Romer, A. S. (1956). Osteology of the Reptiles. Malabar: Krieger Publishing Company.
- Shang, Y., Dong, J. L., Inthavong, K., & Tu, J. Y. (2017). Computational fluid dynamics analysis of wall shear stresses between human and rat nasal cavities. *European Journal of Mechanics B/Fluids*, 61, 160–169.
- Sosnowski, M., Krzywanski, J., Grabowska, K., & Gnatowska, R. (2018). Polyhedral meshing in numerical analysis of conjugate heat transfer. EPJ Web of Conferences, 180, 2096.
- Speigel M, Redel T, Zhang J, Struffert T, Hornegger J, Grossman RG, Doerfler A, Karmonik C. 2009. Tetrahedral and polyhedral mesh evaluation for cerebral hemodynamic simulation – A comparison. Annual International Conference of the IEEE Engineering in Medicine and Biology Society (pp. 2787– 2790).
- Swift, D. L. (1982). Physical principles of airflow and transport phenomena influencing air modification. In D. F. Proctor & I. Anderson (Eds.), *The nose, upper airway physiology and the*

- atmospheric environment (pp. 337-349). Elsevier Science Publishers.
- Takahashi, R. (1987). Review of the Literature on the origin and evolution of the nasal septum. *Acta Oto-Laryngologica*, 104, 70–120.
- Vieira, L. G., Santos, A. L. Q., Lima, F. C., Mendonca, S. H. S. T., Menezes, L. T., & Sebben, A. (2016). Osteologia de Melanosuchus Niger (Crocodylia: Alligatoridae) e a evidencia evolutiva. Pesquisa Veterinaria Brasileira, 36(10), 1025–1044.
- Vogel, S. (1994). Life in moving fluids (2nd ed.). Princeton University Press.
- von Békésy, G. (1964). Olfactory analogue to directional hearing. *Journal of Applied Physiology*, 19(3), 369–373.
- Whitaker, R., & Whitaker, N. (2008). Who's got the biggest? *CSG Newsletter*, 27(4), 26–30.
- Witmer, L. M. (1995). Homology of facial structures in extant archosaurs (birds and crocodilians), with special reference to paranasal pneumaticity and nasal conchae. *Journal of Morphology*, 225, 269–327.

How to cite this article: Bourke, J. M., Fontenot, N., & Holliday, C. (2021). Septal deviation in the nose of the longest faced crocodylian: A description of nasal anatomy and airflow in the Indian gharial (*Gavialis gangeticus*) with comments on acoustics. *The Anatomical Record*, 1–21. https://doi.org/10.1002/ar.24831